

Cavity quantum chromodynamics

T. H. Hansson and R. L. Jaffe

Center for Theoretical Physics, Laboratory for Nuclear Science and Department of Physics,
Massachusetts Institute of Technology, Cambridge, Massachusetts 02139

(Received 12 October 1982)

We develop practical and rigorous techniques for calculating and renormalizing loop diagrams in quantum chromodynamics defined in a static spherical cavity. Working with Feynman propagators and in the Feynman gauge, we use multiple-reflection expansions for the cavity propagators to isolate and analyze the short-distance singularities in graphs. Nonsingular contributions to graphs are evaluated using a set of "Feynman rules" in an energy—angular-momentum representation. As an application we describe the calculation of the quark self-energy to lowest order in α_s . We show that the self-energy of a confined massless quark is finite and unambiguous, and that all divergences in the case of a massive quark can be absorbed into a state-independent mass renormalization just as in free space.

I. INTRODUCTION

The aim of this paper is to develop practical but rigorous techniques for calculating and renormalizing loop diagrams in gauge field theories defined in a static spherical cavity. Typical diagrams of interest are shown in Fig. 1, where the external lines are cavity wave functions and the propagators are "cavity propagators" which satisfy (linear, homogeneous) confining boundary conditions, typically those of the MIT bag model.¹

The diagrams of Fig. 1 are important for phenomenological calculations in QCD using the static-spherical-cavity approximation to the bag model.² $O(\alpha_s)$ corrections to hadron masses, electromagnetic moments, and weak charges require calculation of such diagrams. More generally, to establish a connection between perturbative QCD as applied to deep-inelastic processes at large Q^2 and confinement phenomenology at low Q^2 , one must understand renormalization and renormalization-group evolution in field theories subject to confining boundary conditions. We do not address the question of how well the static spherical cavity approximates the bag model. There are well-known difficulties: the cavity approximation ignores the "quadratic boundary condition" and violates translation invariance. Here we are interested in the very well-defined problem of the structure of (gauge) field theories in finite domains.

Cavity diagrams are harder to compute than ordinary Feynman graphs for several reasons. First, cavity propagators are more complicated. Lacking translation invariance, they depend explicitly on two spatial vectors, \vec{x} and

\vec{x}' , and can only be expressed as infinite sums. Secondly, the constraints of angular momentum conservation at vertices are weaker and algebraically more complex than those of momentum conservation. Finally, the short-distance singularities of the cavity perturbation theory appear at first sight to be worse than those of ordinary perturbation theory, where Lorentz invariance limits divergences to those which can be canceled by Lorentz-invariant Lagrangian counterterms. The allowed divergences of cavity perturbation theory are richer [they can be enumerated by including the timelike unit vector $\eta^\mu = (1,0,0,0)$ in the counterterm Lagrangian]. Furthermore, the sharp boundary which defines the cavity looks like a potential source of such additional short-distance singularities. "Soft" bag models,^{3,4} which smooth out the bag surface, may avoid these surface divergences. However, such models do not lend themselves to practical calculations for several reasons. First, a smooth boundary necessitates much more complicated surface-dependent wave functions and propagators. Second, one could only trust those results which are reasonably insensitive to the details of the smoothing process. Third, by introducing a scalar field with a spatially varying vacuum expectation value to generate the soft bag, one invariably couples this field to the quarks or gluons in a nonrenormalizable fashion⁵ to achieve confinement. Loop-graph calculations are therefore either divergent or dependent on *ad hoc* model assumptions. We will keep the surface sharp and argue that, to lowest nontrivial order, *no new divergences* (beyond those of ordinary perturbation theory) *arise* in physical quantities like energy shifts.

The problem of constructing a practical confined perturbation theory for QCD has been attacked many times in the past.^{4,6-10} Our approach differs in several crucial ways from all previous attempts. First, we separate out the singular parts of all diagrams, and treat them analytically with the methods of conventional renormalization theory; and second, we express the finite parts of diagrams in a form amenable to highly convergent numerical computation. In pursuit of these goals we have employed

(1) Feynman (as opposed to time-ordered) perturbation theory, to reduce the number of graphs in each order;

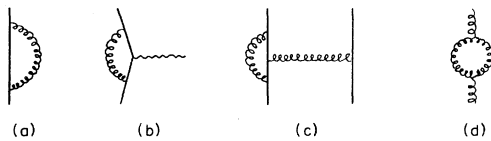


FIG. 1. Examples of cavity perturbation theory diagrams. Solid and spiraled lines denote confined quarks and gluons, respectively, while the wavy line is an (unconfined) photon.

(2) a covariant (namely Feynman) gauge, to simplify the structure of divergences, to avoid ambiguities and spurious singularities associated with noncovariant gauges;

(3) the “multiple-reflection expansion” (MRE) for cavity propagators, to isolate and analyze potential short-distance divergences;

(4) momentum-space techniques, to analyze the most divergent parts of Feynman diagrams (those generated by the two first terms in the MRE);

(5) the rotational invariance of the spherical cavity, to write Feynman rules in angular momentum space with simplifications analogous to the use of momentum space in ordinary perturbation theory; and finally,

(6) Wick rotation, to replace slowly convergent “mode sums” by highly convergent integrals. Some of these elements, notably (1), (5), and (6), appear in other cavity QCD calculations. None alone is of much significance [except perhaps (3)]. Together they enable us to renormalize and calculate with cavity QCD.

Each of these ingredients warrants some discussion.

(1) In the end we find that cavity perturbation theory resembles ordinary perturbation theory very closely: it is vastly more economical to use Feynman propagators than to analyze separately all time-ordered graphs.^{7,8}

(2) Similarly, renormalization is much simpler in covariant gauges than in physical gauges. This is true of proofs to all orders (which we do not attempt here) as well as of the renormalization of one-loop graphs (as discussed in Sec. VI). Another reason we choose a covariant gauge is to avoid the special treatment required for the instantaneous Coulomb propagator in the Coulomb gauge.⁴ This point is discussed further in Appendix A.

(3) We use the multiple-reflection expansion (MRE) to isolate and analyze the short-distance singularities of cavity propagators. The idea of the MRE is very simple and physical¹¹: The propagation from \vec{x} to \vec{x}' in a cavity can be imagined to occur either directly or via any number of reflections from the surface as depicted in Fig. 2. Each line in Fig. 2 is a free propagator $G^0(x, x')$. Here x and x' are four-vectors. The confined propagator $G(x, x')$ can be developed in an expansion in the number of reflections from the surface, schematically

$$\begin{aligned} G(x, x') &= G^0(x, x') + \int ds_\alpha G^0(x, \alpha) G^0(\alpha, x') \\ &+ \int ds_\alpha ds_\beta G^0(x, \alpha) G^0(\alpha, \beta) G^0(\beta, x') \\ &+ \dots, \end{aligned}$$

where α, β, \dots are points on the surface. This is shown pictorially in Fig. 3, where the vertices symbolize reflections. If we interpret reflections as interactions with a dynamical background field describing the vacuum, Fig. 3

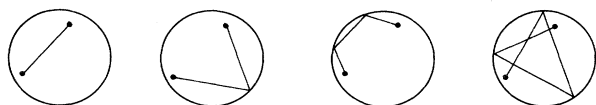


FIG. 2. Pictorial representation of the zero-, one-, two-, and three-reflection contribution to the multiple-reflection expansion for a confined propagator.



FIG. 3. The multiple reflection “Dyson-Schwinger” equation for a confined propagator.

becomes an expansion of the Dyson equation for a soft-bag propagator.

The virtue of the multiple-reflection expansion (for our purposes) is that successive terms are successively less singular at short distances. The divergent parts of the Feynman graphs we have studied involve at most one reflection. We show explicitly that all divergences in the lowest-order (in α_s) fermion self-energy lie in the zero-reflection term, and can be renormalized exactly as in the continuum. To the same order the (off-shell) propagator insertion has divergences also in the one-reflection term, while higher reflections remain finite. Thus the MRE provides an extremely powerful tool for cavity perturbation theory: it allows us to regulate and renormalize cavity Feynman graphs using the familiar techniques of ordinary perturbation theory.

An important aspect of the MRE is the decomposition of the propagator into a free term, $G^0(x, x')$, and a boundary term, $\tilde{G}(x, x')$,

$$G(x, x') = G^0(x, x') + \tilde{G}(x, x'),$$

where $\tilde{G}(x, x')$ obeys the homogeneous equation and is adjusted so $G(x, x')$ obeys the proper boundary condition.

For arbitrary geometries $\tilde{G}(x, x')$ cannot be obtained in closed form. For a sphere, with the aid of rotational symmetry, it can. Constructing \tilde{G} is equivalent to resumming all terms in the MRE except the first (zeroth reflection). Alternatively, one can keep the zeroth and first reflection and resum the rest,

$$\begin{aligned} G(x, x') &= G^0(x, x') + \int ds_\alpha G^0(x, \alpha) G^0(\alpha, x') \\ &+ \Gamma(x, x'). \end{aligned}$$

These alternatives give us great flexibility. We can separate out any number of singular terms in a propagator for special, analytic treatment, and then resum the rest for convenient numerical evaluation.

Numerical calculations are simplest when all but the first one or two terms in the MRE are resummed. Nevertheless, it is important to study the contribution to physical quantities from successive reflections since this indicates which depend weakly on the details of confinement and which strongly.

(4) The most divergent contribution to any Feynman diagram is generated by taking the zeroth-reflection contribution to all the propagators. Except for external wavefunction factors, this contribution does not “know” about the surface and is translationally invariant, and can be evaluated in momentum space using conventional Feynman rules. Computation is simple, since we can borrow standard techniques for handling divergences in momentum space. Also, we can be confident that the regularization scheme we use does not violate the generalized Ward identities which are crucial in order to obtain cancellation of divergences and to preserve gauge invariance after renormalization.

Momentum-space techniques also simplify the analysis of loop diagrams with first-reflection terms in one or more propagators. The leading short-distance singularities in the first-reflection terms are the same as the ones generated by an infinite plane and are most easily handled by going to momentum space in the directions tangent to the plane. Using this mixed (x, \vec{p}_\perp) representation, we will prove that the first-reflection contributions to the lowest-order quark self-energy are finite.

(5) Rotational invariance plays a role in our formalism analogous to Poincaré invariance in unconfined field theories. Manifest rotational covariance, via the Wigner-Eckart theorem (and its generalization to four-point functions), fixes the structure of our vertices. Loop summations over angular momenta replace the loop momentum integrations of unconfined theories. In this aspect our approach resembles that of Refs. 7 and 9, where the importance of manifest rotational covariance was also recognized. We achieve considerable additional simplification, however, by making an $SU(2) \times SU(2)$ decomposition of the Dirac field. This allows us to handle the rotational properties of the Dirac field in precisely the same manner as scalar or vector fields, and considerably reduces the number of invariant matrix elements describing the quark-gluon vertex.

(6) In the end, the finite parts of loop graphs are given by multidimensional integrals over the frequencies (energies) of internal lines and the radial coordinates of interaction vertices, and multidimensional sums over angular momenta. The integrands have singularities at (real) values of the energy corresponding to all confined cavity eigenstates. Calculation of this integral by the method of residues would reduce to a multidimensional sum over cavity eigenstates ("modes"). Such sums are cumbersome, and slowly convergent.^{6,7} We avoid them by performing a Wick rotation.^{8,10} For the quark self-energy, we show it is possible to rotate the energy integral until it is parallel to the imaginary axis. The resulting multidimensional integral is highly convergent.

Our intention in this paper is pedagogical: We spell out many of the details for scalar, spinor, and vector fields. We assume the reader is well versed in ordinary Feynman perturbation theory but has little or no familiarity with confined field theories or with the multiple-reflection expansion. Although most of the results for scalars are not new and, indeed, some are elementary, we review them in detail in the next section as a warmup for the spinor and vector problem. We derive closed expressions for the scalar propagator subject to Dirichlet or Neumann boundary conditions in a partial-wave expansion, and discuss their analytic structure. We introduce the MRE, study its convergence as a function of complex frequency, and show how to resum it. We then study the singularity structure of the MRE, and show how to isolate interior and surface singularities. In Secs. III and IV, we repeat the analysis for Dirac, vector, and ghost fields. The propagator for the Dirac field confined to a spherical cavity was first written down by Bender and Hayes¹² in much the same form as we employ it. It also appears in the work of Milton.¹³ The MRE for confined fermions was first used in Ref. 14. The extension to confined vectors is, to our knowledge, new, although the case of conducting boundary conditions

has been studied previously.¹⁵ In Sec. V, we study the vertices of quantum chromodynamics and combine with this the results of Secs. III and IV into a set of "Feynman rules" for confined QCD.

Finally, in Sec. VI, we illustrate our methods by describing the renormalization and calculation of the self-energy of a confined quark to one-loop order in QCD. In most of this paper we limit ourselves to massless quarks. In Sec. VI, however, we also discuss the self-energy of a massive quark. We show that it diverges logarithmically and show that the divergence can be absorbed into a state-independent mass renormalization. The renormalized quark mass m depends on an arbitrary renormalization point μ in precisely the same way as it happens in free space. After handling the divergences generated by the zeroth-reflection terms, we then show that higher reflections are finite and finally give an expression for the quark self-energy which can be put on the computer. Section VI also contains some remarks on the calculation and renormalization of the confined gluon self-energy to one-loop order.

The reader may wish to consult Sec. VI for a preview of our methods before going into the details of cavity perturbation theory.

In the interest of brevity, we have omitted proofs of many assertions regarding the multiple-reflection expansion. Since the MRE is of interest in itself and since some of our results are novel, we have assembled them into a separate paper on the MRE.¹⁶

II. THE SCALAR FIELD

A. The cavity propagator

We define the "cavity propagator" in a confined quantum field theory to be the Green's function of the equation of motion including boundary conditions, but ignoring interactions. For a massless scalar field,

$$\square \Delta(x, x') = -\delta^4(x - x'), \quad (2.1)$$

where $\square = \partial_0^2 - \nabla^2$, $x = (t, \vec{x})$. We take the Feynman boundary conditions at $t = \pm \infty$. In addition, it is necessary to impose boundary conditions on the surface of the spherical cavity of radius R to which the fields are confined.

For the scalar field we consider two different boundary conditions:

$$\text{Dirichlet: } \Delta^D(x, x') \big|_{\vec{x} = \vec{\alpha}} = 0 \quad (2.2a)$$

and

$$\text{Neumann: } \hat{x} \cdot \vec{\nabla} \Delta^N(x, x') \big|_{\vec{x} = \vec{\alpha}} = 0. \quad (2.2b)$$

Three-vectors on the surface of the sphere are denoted henceforth by $\vec{\alpha}$, $\vec{\beta}$, etc., while \vec{x}, \vec{y}, \dots are interior vectors. Analogous conditions are imposed when \vec{x}' is on the boundary. The generalization to "mixed" boundary conditions is straightforward and is given in Sec. IV, where it is required.

There are many representations for the propagator $\Delta(x, x')$. The form most often used in studies of confined QCD has been the eigenfunction expansion or mode sum. This is not a convenient representation in which to handle

the short-distance singularities of perturbation theory. Instead we decompose the cavity propagator into a free-space propagator and a boundary term

$$\Delta(x, x') = \Delta^0(x, x') + \tilde{\Delta}(x, x'), \quad (2.3)$$

where $\Delta^0(x, x')$ is the free, scalar Feynman propagator. $\tilde{\Delta}(x, x')$ obeys the homogeneous equation analogous to Eq. (2.1) and is adjusted so $\Delta(x, x')$ obeys Eqs. (2.2a) or (2.2b).

The decomposition of Δ into a free part and a boundary part can be made (and exploited) independent of the shape of the cavity. In order to obtain explicit representations for Δ^0 and $\tilde{\Delta}$, we exploit the symmetries of the sphere: time translation and rotational invariance. We transform to frequency space,

$$\Delta(\vec{x}, \vec{x}', \omega) = \int dt e^{i\omega(t-t')} \Delta(x, x'), \quad (2.4)$$

and perform a partial-wave expansion

$$\Delta(\vec{x}, \vec{x}', \omega) = \sum_{lm} \Delta_l(r, r', \omega) Y_{lm}(\Omega) Y_{lm}^*(\Omega'). \quad (2.5)$$

The partial-wave propagator, $\Delta_l(r, r', \omega)$, satisfies

$$\left[\frac{1}{r} \frac{\partial^2}{\partial r^2} r - \frac{l(l+1)}{r^2} + \omega^2 \right] \Delta_l(r, r', \omega) = \frac{\delta(r-r')}{rr'} \quad (2.6)$$

and

$$\Delta_l^D(R, r'; \omega) = 0 \quad (2.7a)$$

or

$$\left. \frac{\partial}{\partial r} \Delta_l^N(r, r', \omega) \right|_{r=R} = 0. \quad (2.7b)$$

$$\Delta^D(\vec{x}, \vec{x}', \omega) = -i\omega \sum_{lm} \left[j_l(\omega r_<) h_l^{(1)}(\omega r_>) - \frac{h_l^{(1)}(x)}{j_l(x)} j_l(\omega r) j_l(\omega r') \right] Y_{lm}(\Omega) Y_{lm}^*(\Omega'), \quad (2.12a)$$

$$\Delta^N(\vec{x}, \vec{x}', \omega) = -i\omega \sum_{lm} \left[j_l(\omega r_<) h_l^{(1)}(\omega r_>) - \frac{h_l^{(1)'}(x)}{j_l'(x)} j_l(\omega r) j_l(\omega r') \right] Y_{lm}(\Omega) Y_{lm}^*(\Omega') \quad (2.12b)$$

for $\text{Im}\omega > 0$. For $\text{Im}\omega < 0$, i is replaced by $-i$ and $h_l^{(1)}$ by $h_l^{(2)}$.

B. The analytic structure of the propagator

The partial-wave cavity propagator, Δ_l , and the free propagator, Δ_l^0 , are both real analytic functions of ω , i.e., they satisfy the Schwartz reflection relation

$$\begin{aligned} \Delta_l^0(r, r', \omega)^* &= \Delta_l^0(r, r', \omega^*), \\ \Delta_l(r, r', \omega)^* &= \Delta_l(r, r', \omega^*) \end{aligned} \quad (2.13)$$

with singularities on the real axis at values of ω which are eigenvalues of the corresponding Hamiltonian.

The free partial-wave propagator has a cut on the entire real axis associated with a continuum of unconfined positive- and negative-energy eigenstates. The discontinuity across the cut is

$$\begin{aligned} \Delta_l^0(r, r', \omega_0 + i\epsilon) - \Delta_l^0(r, r', \omega_0 - i\epsilon) \\ = -2i\omega_0 j_l(\omega_0 r) j_l(\omega_0 r'), \end{aligned} \quad (2.14)$$

Now decompose Δ_l in analogy to Eq. (2.3),

$$\Delta_l(r, r', \omega) = \Delta_l^0(r, r', \omega) + \tilde{\Delta}_l(r, r', \omega). \quad (2.8)$$

The free partial-wave propagator, $\Delta_l^0(r, r', \omega)$, is constructed by direct integration of Eq. (2.6):

$$\begin{aligned} \Delta_l^0(r, r', \omega) &= -i\omega j_l(\omega r_<) h_l^{(1)}(\omega r_>), \quad \text{Im}\omega > 0 \\ &= i\omega j_l(\omega r_<) h_l^{(2)}(\omega r_>), \quad \text{Im}\omega < 0. \end{aligned} \quad (2.9)$$

The normalization of $\Delta_l^0(r, r', \omega)$ is determined by the jump condition at $r=r'$ in Eq. (2.6). Finally, the Feynman boundary conditions at $t=\pm\infty$ prescribe the way in which $\Delta_l^0(r, r', \omega)$ is to be interpreted on the real axis (where it has a cut). A complete discussion of the analytic structure of Δ_l^0 and Δ_l is given later in this section.

$\tilde{\Delta}_l(r, r', \omega)$ is a solution to the homogeneous equation analogous to Eq. (2.6). It is regular at $r=0$ and $r'=0$ and symmetric in $r \leftrightarrow r'$. It must therefore be of the form

$$\tilde{\Delta}_l^{D(N)}(r, r', \omega) = i\omega a_l^{D(N)} j_l(\omega r) j_l(\omega r'), \quad (2.10)$$

where $a_l^{D(N)}$ must be chosen to satisfy the Dirichlet (D) or Neumann (N) boundary conditions, Eq. (2.7a) or (2.7b), whence

$$a_l^D = h_l^{(1)}(x) / j_l(x), \quad (2.11a)$$

$$a_l^N = h_l^{(1)'}(x) / j_l'(x) \quad (2.11b)$$

for $\text{Im}\omega > 0$, where $x \equiv \omega R$. For $\text{Im}\omega < 0$, $h_l^{(1)}$ is replaced by $-h_l^{(2)}$.

To summarize, the Dirichlet and Neumann scalar cavity propagators are given by

where ω_0 is real. According to the Feynman boundary conditions at $t=\pm\infty$ the physical propagator for real ω is given by the limit as ω approaches the real axis from above for $\text{Re}\omega > 0$ and from below for $\text{Re}\omega < 0$. This is represented in Fig. 4 by displacing the cuts slightly below and above the real axis, respectively.

The full cavity partial-wave propagator, on the other hand, must be a meromorphic function of ω in the complex plane, with poles at the (discrete) eigenvalues of the cavity Hamiltonian. To make this explicit we rewrite Δ_l using

$$h_l^{(1)'}(x) = j_l(x) \pm i n_l(x) \quad (2.15)$$

so

$$\begin{aligned} \Delta_l^D(r, r', \omega) &= \omega j_l(\omega r_<) n_l(\omega r_>) \\ &\quad - \omega \frac{n_l(x)}{j_l(x)} j_l(\omega r) j_l(\omega r'), \end{aligned} \quad (2.16a)$$

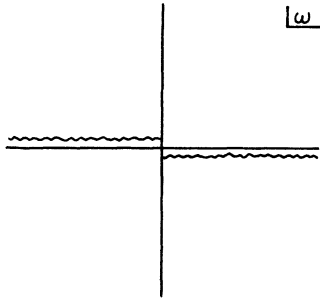


FIG. 4. Position of the cuts in the complex ω plane for Δ_l^0 as given by Eq. (2.9).

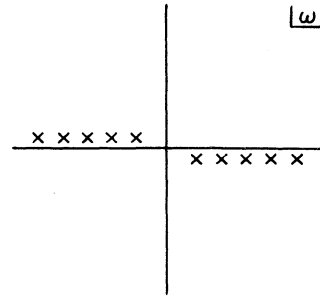


FIG. 5. Position of the poles in the complex ω plane for Δ^D and Δ^N as given by Eqs. (2.12).

$$\Delta_l^N(r, r', \omega) = \omega j_l(\omega r_<) n_l(\omega r_>) - \omega \frac{n_l'(x)}{j_l'(x)} j_l(\omega r) j_l(\omega r') \quad (2.16b)$$

for all ω . $\Delta_l^{D(N)}(r, r', \omega)$ is analytic everywhere except at the zeros of $j_l(x)$ [$j_l'(x)$], which are the eigenvalues of the scalar Dirichlet (Neumann) problem. The residues at the poles are the properly normalized eigenfunctions of the appropriate Hamiltonian. The Feynman boundary conditions at $t = \pm \infty$ require the singularities in $\Delta_l(r, r', \omega)$ to be displaced: slightly below the real axis for $\text{Re}\omega > 0$ and slightly above for $\text{Re}\omega < 0$. This $i\epsilon$ prescription will always be assumed and is displayed in Fig. 5.

In addition, the Neumann propagator possesses a double pole at $\omega = 0$ with coefficient $3/4\pi R^3$. The same singularity arises in the timelike component of the gluon propagator. Its role (or lack thereof) in cavity perturbation theory is discussed at length in Appendix A.

Finally, we discuss the $|\omega| \rightarrow \infty$ behavior of Δ_l^0 and $\tilde{\Delta}_l$. For definiteness we take $\text{Im}\omega > 0$. The behavior in the lower half plane is similar. Δ_l^0 is exponentially bounded

for large $|\omega|$,

$$\Delta_l^0(r, r', \omega) \sim \frac{-1}{2\omega r r'} e^{i\omega(r_> - r_<)}, \quad \text{Im}\omega > 0 \quad (2.17)$$

except at the point $r = r'$ where it vanishes like $1/\omega$. $\tilde{\Delta}_l$, on the other hand, vanishes exponentially for large $|\omega|$ except when $r = r' = R$:

$$\tilde{\Delta}_l(r, r', \omega) \sim \frac{1}{2\omega r r'} e^{i\omega(2R - r - r')}, \quad \text{Im}\omega > 0. \quad (2.18)$$

This behavior as $\omega \rightarrow \infty$ is good enough to allow us to Wick rotate ω integrations to the imaginary axis.

C. Multiple-reflection expansion

In this and the following section we give a short survey of the multiple-reflection expansion for scalar propagators. For details concerning the MRE in a general cavity we refer to the work of Balian and Bloch¹¹ and to Ref. 16. For derivations of results specific to a sphere (including the resummation described in Sec. IID below), see Ref. 16. The MRE for the Dirichlet propagator is given by

$$\Delta^D(\vec{x}, \vec{x}', \omega) = \Delta^0(\vec{x}, \vec{x}', \omega) - 2R \int d\Omega_\alpha [\partial_\alpha \Delta^0(\vec{x}, \vec{\alpha}, \omega)] \Delta^0(\vec{\alpha}, \vec{x}', \omega) + (2R)^2 \int d\Omega_\alpha d\Omega_\beta [\partial_\alpha \Delta^0(\vec{x}, \vec{\alpha}, \omega)] [\partial_\beta \Delta^0(\vec{\alpha}, \vec{\beta}, \omega)] \Delta^0(\vec{\beta}, \vec{x}', \omega) + \dots \quad (2.19)$$

As before, $\vec{\alpha}$ is a point on the surface and we use a shorthand notation for the radial derivative:

$$\partial_\alpha \Delta^0(\vec{x}, \vec{\alpha}, \omega) \equiv R \frac{\partial}{\partial r'} \Delta^0(\vec{x}, \vec{x}', \omega) \Big|_{\vec{x}' = \vec{\alpha}} \quad (2.20)$$

[Although we consider a sphere, everything in this subsection holds for a general smooth cavity if we replace $R^2 d\Omega_\alpha$ by ds_α and ∂_α by the normal derivative (see Ref. 11).]

Equation (2.20) is not manifestly symmetric in $\vec{x} \leftrightarrow \vec{x}'$, nor is it obvious that it satisfies the Dirichlet condition as \vec{x}' approaches the surface. In fact, it is symmetric and it does satisfy the \vec{x}' -Dirichlet condition. In Ref 16, we show it possible to rewrite Eq. (2.19) term by term in a manifestly symmetric form:

$$\Delta^D(\vec{x}, \vec{x}', \omega) = \Delta^0(\vec{x}, \vec{x}', \omega) - R \int d\Omega_\alpha \Delta^0(\vec{x}, \vec{\alpha}, \omega) \vec{\partial}_\alpha \Delta^0(\vec{\alpha}, \vec{x}', \omega) + R^2 \int d\Omega_\alpha d\Omega_\beta \Delta^0(\vec{x}, \vec{\alpha}, \omega) \vec{\partial}_\alpha \Delta^0(\vec{\alpha}, \vec{\beta}, \omega) \vec{\partial}_\beta \Delta^0(\vec{\beta}, \vec{x}', \omega) - \dots, \quad (2.21)$$

where

$$\vec{f} \vec{\partial}_\alpha g = (\partial_\alpha f)_g + f(\partial_\alpha g). \quad (2.22)$$

A demonstration that Eq. (2.21) satisfies the Dirichlet condition on both \vec{x} and \vec{x}' is given in Ref. 16. We wish to emphasize that the correspondence between Eqs. (2.19) and (2.21) is term by term. Therefore the existence of two forms for

the Dirichlet MRE does not confuse the meaning of the n th reflection. Of course, the usefulness of the MRE depends on whether or not it converges, which we will discuss below. Even if it does not converge it may be useful if the remainder after n terms can be explicitly calculated, which is indeed the case in a sphere.

The Neumann propagator possesses an MRE similar to Eq. (2.21),

$$\begin{aligned} \Delta^N(\vec{x}, \vec{x}', \omega) = & \Delta^0(\vec{x}, \vec{x}', \omega) + R \int d\Omega_\alpha \Delta^0(\vec{x}, \alpha, \omega) \vec{\partial}_\alpha \Delta^0(\vec{\alpha}, \vec{x}', \omega) \\ & + R^2 \int d\Omega_\alpha d\Omega_\beta \Delta^0(\vec{x}, \vec{\alpha}, \omega) \vec{\partial}_\alpha \Delta^0(\vec{\alpha}, \vec{\beta}, \omega) \vec{\partial}_\beta \Delta^0(\vec{\beta}, \vec{x}', \omega) + \dots, \end{aligned} \quad (2.23)$$

the only difference from the Dirichlet case being the signs.

D. Summing the multiple-reflection expansion

Here we show how to relate the expressions for the scalar cavity propagator obtained in the previous two subsections. The key to summing the MRE is that it is diagonal in angular momentum. It simplifies considerably when we substitute the partial-wave expansion [Eqs. (2.5) and (2.9)] for the free propagator and perform all angular integrals. The result is a geometrical series which can be summed to give the correct confined partial-wave propagator Δ_l . Details are given in Ref. 16 and here we only quote the result,

$$\Delta_l^D(r, r', \omega) = -i\omega \left[j_l(\omega r_<) h_l^{(1)}(\omega r_>) + \frac{2ix^2 j_l(\omega r) j_l(\omega r') h_l^{(1)}(x) h_l^{(1)'}(x)}{1 - ix^2 [j_l'(x) h_l^{(1)}(x) + j_l(x) h_l^{(1)'}(x)]} \right] \quad (2.24)$$

for the Dirichlet boundary condition and $\text{Im}\omega > 0$. The multiple-reflection expression for $\Delta_l^D(r, r', \omega)$ is generated, term by term, by making a geometrical expansion of the denominator in the second term of Eq. (2.24). Equation (2.24) reproduces the partial-wave expansion of Δ_l^D [Eq. (2.12a)] when one uses the Wronskian identity

$$j_l(x) h_l^{(1)'}(x) - j_l'(x) h_l^{(1)}(x) = i/x^2. \quad (2.25)$$

The corresponding result for the Neumann propagator is

$$\Delta_l^N(r, r', \omega) = -i\omega \left[j_l(\omega r_<) h_l^{(1)}(\omega r_>) - \frac{2ix^2 j_l(\omega r) j_l(\omega r') h_l^{(1)}(x) h_l^{(1)'}(x)}{1 + ix^2 [j_l'(x) h_l^{(1)}(x) + j_l(x) h_l^{(1)'}(x)]} \right] \quad (2.26)$$

for $\text{Im}\omega > 0$. Any number of reflections can be singled out of either the Dirichlet or Neumann propagator by partial expansion of the denominator in Eqs. (2.24) or (2.26), i.e., denoting the denominator as $1 - z$ and using identities such as

$$\frac{1}{1-z} = 1 + \frac{z}{1-z}, \quad \frac{1}{1-z} = 1 + z + \frac{z^2}{1-z},$$

etc.

Now that the relation between the partial-wave propagator and its multiple-reflection expansion has been made explicit, it is possible to study the convergence of the MRE as a function of x ($=\omega R$). Since the MRE for the Dirichlet [Neumann] boundary conditions is obtained by a geometrical expansion of the denominator in Eq. (2.24) [Eq. (2.26)], both converge if and only if

$$|z_l(x)| < 1. \quad (2.27)$$

Of course, the MRE does not converge at the poles of Δ_l^D where $z_l = 1$. These occur at the isolated, real values of x, x_{nl}^D , at which $j_l(x) = 0$. There are neighborhoods of each pole along the real axis in which the MRE does not converge. Thus the MRE is not a useful expansion for the propagator for real ω . On the other hand, the MRE can be shown to converge everywhere on the imaginary axis. The only exception is the $l=0$ partial wave which does not converge at $\omega=0$. For the Neumann propagator this reflects the double pole at $\omega=0$ (see Appendix A). For the Dirichlet case the MRE does not converge even though the propagator is nonsingular, just as the geometrical expansion of $1/(1-x)$ fails to converge at $x = -1$. We in-

tend to evaluate loop integrations over ω by Wick rotation to the imaginary axis, where the MRE converges everywhere except at $\omega=0$ for the $l=0$ partial wave.

E. Short-distance singularities

In order to analyze the divergences in Feynman graphs, we must study the short-distance behavior of the confined propagators. The MRE is ideally suited for this purpose. This discussion does not rely on the convergence of the MRE since it is always possible to single out any finite number of reflections, and sum the rest analytically.

First, however, we must make clear what is to be meant by short-distance behavior. We are interested in the ultraviolet (UV) behavior of confined Feynman graphs. In momentum space UV singularities can be discovered simply by counting powers of loop momenta. In (\vec{x}, ω) space, the UV singularities show up as small $|\vec{x} - \vec{x}'|$ and large ω_{loop} divergences. We must therefore study leading terms in $1/|\vec{x} - \vec{x}'|$ and ω . In particular, a term $\sim \omega |\vec{x} - \vec{x}'|$ is considered as $O(1)$. In the following discussion, short distance always refer to this limit of small spatial distances and large energies.

For \vec{x} and \vec{x}' away from the surface, the only singularity is the usual $1/|\vec{x} - \vec{x}'|$ divergence in the zero-reflection term. When both \vec{x} and \vec{x}' approach the surface new singularities are encountered. First consider the one-reflection term

$$\begin{aligned} \Delta^1(\vec{x}, \vec{x}', \omega) = & \mp 2R \int d\Omega_\alpha \Delta^0(\vec{x}, \vec{\alpha}, \omega) \\ & \times \partial_\alpha \Delta^0(\vec{\alpha}, \vec{x}', \omega), \end{aligned} \quad (2.28)$$

where the upper and lower signs refer to the Dirichlet and Neumann boundary conditions, respectively. Close enough, the spherical surface looks like a plane, so to extract the leading short-distance singularity in Eq. (2.28), we consider the corresponding equation for the half-space (HS) $x_1 < 0$:

$$\Delta_{HS}^1(\vec{x}, \vec{x}', \omega) = \mp 2 \int_{x_1''=0} d^2x_1 \Delta^0(\vec{x}, \vec{x}'', \omega) \times \frac{\partial}{\partial x_1''} \Delta^0(\vec{x}'', \vec{x}', \omega), \quad (2.29)$$

where $\vec{x}_1 = (x_2, x_3)$. It is convenient to go to Fourier space in the variable \vec{x}_1 and also rotate to imaginary energy $\omega = ip_4$. The free propagator then becomes

$$\Delta^0(x_1, x_1', \vec{p}_1, p_4) = \Delta^0(x_1 - x_1', \vec{p}) = -\frac{1}{2} \frac{e^{-|x_1 - x_1'| |\vec{p}|}}{|\vec{p}|}, \quad (2.30)$$

where $\vec{p} = (\vec{p}_1, p_4)$. In this representation, the integral in Eq. (2.29) becomes a product, and one obtains

$$\Delta_{HS}^1(x_1, x_1', \vec{p}) = \mp \Delta^0(x_1 + x_1', \vec{p}) \quad (2.31)$$

or, back in (\vec{x}, ω) space,

$$\Delta_{HS}^1(\vec{x}, \vec{x}', \omega) = \mp \Delta^0(\vec{x}, \vec{x}'_R, \omega), \quad (2.32)$$

where

$$\vec{x}_R = \vec{x}_1 - x_1 \hat{x}_1. \quad (2.33)$$

This result is easily understood. The point \vec{x}'_R is the image point of \vec{x}' , so the one-reflection term in the MRE simply corresponds to direct propagation from the image charge. For an infinite plane, this is the whole story; for a curved surface Eq. (2.32) gives the leading singular behavior close to the surface.

Going back to the spherical geometry, it is useful to introduce the following variables:

$$\xi = \frac{2R - r - r'}{R}, \quad (2.34a)$$

$$\eta = \frac{r - r'}{R}. \quad (2.34b)$$

If the angle between \vec{x} and \vec{x}' is θ and we make the approximation $\sin\theta \simeq \theta$, the zero- and one-reflection terms for both \vec{x} and \vec{x}' close to the surface are now given by¹⁷

$$\Delta^0(\vec{x}, \vec{x}', \omega) \simeq -\frac{1}{4\pi R} \frac{e^{ix(\eta^2 + \theta^2)^{1/2}}}{(\eta^2 + \theta^2)^{1/2}} \quad (2.35)$$

and

$$\Delta^1(\vec{x}, \vec{x}', \omega) \simeq \mp \frac{1}{4\pi R} \frac{e^{ix(\xi^2 + \theta^2)^{1/2}}}{(\xi^2 + \theta^2)^{1/2}}, \quad (2.36)$$

where $x = \omega R$ and $\text{Im}\omega > 0$. From Eq. (2.36) one sees that the one-reflection term is singular only when the two points coincide and simultaneously reach the surface. The above singularities in Δ^0 and Δ^1 are the only ones that will be important in calculating (one-) loop diagrams although, as will be seen below, there is also a logarithmic singularity in the two-reflection term.

To analyze the short-distance singularities of higher re-

flection terms, we apply the addition theorem for spherical harmonics in Eq. (2.5),

$$\Delta(\vec{x}, \vec{x}', \omega) \equiv \Delta(r, r', \cos\theta, \omega) = \sum_{l=0}^{\infty} \frac{2l+1}{4\pi} P_l(\cos\theta) \Delta_l(r, r', \omega). \quad (2.37)$$

The l summation converges except when both $\cos\theta = 1$ and $r = r'$. The analysis is especially easy when r and r' are on the same ray and ω is kept fixed. (This means that we do not explore the complete UV divergence. For this we must resort to the previous formulas. For demonstrating the presence of a logarithmic singularity in Δ^2 , however, the partial-wave method is convenient and sufficient.) Thus we study the singularities by setting $\cos\theta = 1$ and exploring the singular behavior of $\Delta(r, r', 1, \omega)$ for $r \sim r'$. Since the singularities arise as divergences in the l summation, we use the large- l asymptotic expansions for the spherical Bessel functions.

Consider first the free propagator, $\Delta^0(r, r', 1, \omega)$. Upon substituting the asymptotic forms of j_l and n_l , we obtain

$$\Delta^0(r, r', 1, \omega) \sim -\frac{1}{4\pi |r - r'|}, \quad (2.38)$$

which coincides with Eq. (2.35) if we take $\theta = 0$ and drop terms $\sim \eta x$.

Next consider the boundary term for the Dirichlet propagator (the Neumann propagator behaves similarly). The same analysis gives

$$\tilde{\Delta}^D(r, r', 1, \omega) \sim \frac{R}{4\pi(R^2 - rr')}, \quad (2.39)$$

which has a linear singularity only when both r and r' approach R . The same approach allows us to analyze the successive reflection terms contributing to $\tilde{\Delta}^D$. From Eq. (2.24), we obtain the n th reflection,

$$\Delta^{D,n}(r, r', 1, \omega) = 2\omega x^2 \sum_{l=0}^{\infty} \frac{2l+1}{4\pi} j_l(\omega r) j_l(\omega r') \times h_l^{(1)}(x) h_l^{(1)'}(x) [z_l(x)]^{n-1} \quad (2.40)$$

for $\text{Im}\omega > 0$. Extracting asymptotic behavior in the same manner, we find

$$\Delta^{D,1}(r, r', 1, \omega) \sim \frac{R}{4\pi(R^2 - rr')}, \quad (2.41)$$

$$\Delta^{D,2}(r, r', 1, \omega) \sim +\frac{1}{8\pi R} \ln \left[1 - \frac{rr'}{R^2} \right], \quad (2.42)$$

and $\Delta^{D,n}(r, r', 1, \omega)$ is finite for $n > 2$. Equation (2.41) coincides with Eq. (2.36) if we put $\theta = \xi x = 0$. Apparently the dominant (linear) surface singularity of $\tilde{\Delta}^D$ is generated entirely by the first reflection.

The utility of the multiple-reflection expansion is now apparent: it is an expansion in decreasingly singular behavior at short distances. We should mention that the propagator $\Delta^D(\vec{x}, \vec{x}', \omega)$ will typically appear multiplied by expressions involving wave functions which vanish linearly on the boundary. Thus the surface singularities in $\tilde{\Delta}^D$ do not generate new divergences in Feynman graphs.

III. THE DIRAC FIELD

A. The cavity propagator

In this section, we analyze the confined Dirac propagator in the same fashion as the scalar propagator was analyzed in the previous section. Some technical details which arise in this section are relegated to Appendix B. The cavity propagator for a massless Dirac field obeys

$$(\gamma^0\omega + i\vec{\gamma}\cdot\vec{\nabla})S(\vec{x}, \vec{x}', \omega) = \delta^3(\vec{x} - \vec{x}') \quad (3.1)$$

and

$$(i\vec{\gamma}\cdot\hat{\alpha} + 1)S(\vec{\alpha}, \vec{x}', \omega) = 0, \quad (3.2)$$

where $\vec{\alpha}$ is on the boundary. An analogous condition holds when \vec{x}' is on the boundary. Throughout this section we take $\text{Im}\omega > 0$, unless otherwise stated. The analytic continuation to $\text{Im}\omega < 0$ is more complicated for the Dirac propagator and is discussed below. To exploit rotational invariance most fully, we decompose the Dirac spinor space into a direct product of SU(2) spaces, ρ space and σ space, defined by

$$\gamma^0 = \rho^3 \otimes 1, \quad (3.3a)$$

$$\vec{\gamma} = i\rho^2 \otimes \vec{\sigma}, \quad (3.3b)$$

$$\gamma^5 = \rho^1 \otimes 1, \quad (3.3c)$$

where $\vec{\rho}$ and $\vec{\sigma}$ are Pauli matrices. In terms of $\vec{\rho}$ and $\vec{\sigma}$, Eqs. (3.1) and (3.2) become

$$(\rho^3\omega - \rho^2\vec{\sigma}\cdot\vec{\nabla})S(\vec{x}, \vec{x}', \omega) = \delta^3(\vec{x} - \vec{x}') \quad (3.4)$$

and

$$(\rho^2\vec{\sigma}\cdot\hat{\alpha} - 1)S(\vec{\alpha}, \vec{x}', \omega) = 0 \quad (3.5)$$

on the boundary.

$S(\vec{x}, \vec{x}', \omega)$ may be expanded in partial waves employing the two-component spinor spherical harmonics $\phi_{jlm}^\alpha(\Omega)$ (the spinor index α generally will be suppressed),

$$S(\vec{x}, \vec{x}', \omega) = \sum_{jll'm} S_{jll'm}(r, r', \omega) \phi_{jlm}(\Omega) \phi_{j'l'm}^\dagger(\Omega'), \quad (3.6)$$

where $S_{jll'm}$ is a 2×2 matrix in ρ space. The lack of coupling between the angular and the ρ -space dependences of Eq. (3.6) reflects the fact that the generators of rotations of a Dirac spinor commute with all ρ -space transformations. S is not diagonal in l since orbital angular momentum is not conserved by the Dirac Hamiltonian. The sums on j , l , and m carry the usual restrictions: $j = \frac{1}{2}, \frac{3}{2}, \frac{5}{2}, \dots$, $l = j \pm \frac{1}{2}$ and $-j \leq m \leq j$. To obtain a set of equations for the partial-wave propagators, $S_{jll'm}$, we also need the completeness condition

$$\delta^{\alpha\beta}\delta^2(\Omega - \Omega') = \sum_{jlm} \phi_{jlm}^\alpha(\Omega) \phi_{jlm}^\dagger{}^\beta(\Omega'). \quad (3.7)$$

$S_{jll'm}$ can be decomposed into the free partial-wave propagator plus a boundary term

$$S_{jll'm}(r, r', \omega) = S_{jll'm}^0(r, r', \omega) + \tilde{S}_{jll'm}(r, r', \omega). \quad (3.8)$$

We obtain $S_{jll'm}^0$ from the differential equations and boundary conditions which define the free, Feynman propagator. This analysis is carried out in Appendix B. The result, for $\text{Im}\omega > 0$, is

$$S_{jll'm}^0(r, r', \omega) = -i\omega^2 [\delta_{l,l'}\rho^3 + (l' - l)\rho^2] f_l(\omega r) f_{l'}(\omega r'). \quad (3.9)$$

The functions $f_l(\omega r)$ are defined as follows:

$$f_l(\omega r) = j_l(\omega r)\theta(r' - r) + h_l^{(1)}(\omega r)\theta(r - r'). \quad (3.10)$$

Strictly speaking, our notation here is not correct, since f_l is a function of two variables. However, only the combination $f_l(r)f_{l'}(r')$ occurs so there should be no confusion, and what we have lost in precision we have gained in compactness and simplicity.

The boundary term $\tilde{S}_{jll'm}$ must be of the form

$$\tilde{S}_{jll'm}(r, r', \omega) = i\omega^2 \tilde{a}_{jll'm}(x) j_l(\omega r) j_{l'}(\omega r'), \quad (3.11)$$

where $x = \omega R$, in order to satisfy the differential equations and regularity requirements. The coefficients $\tilde{a}_{jll'm}$ are 2×2 matrices in ρ space which must be chosen to satisfy the boundary condition Eq. (3.5). Once again details may be found in Appendix B. The results for $\text{Im}\omega > 0$ is

$$\tilde{S}_{jll'm}(r, r', \omega) = i\omega^2 \{c_j(x) [\delta_{ll'}\rho^3 + (l' - l)\rho^2] + d_j(x) [(\bar{l} - l)\delta_{ll'} - i\delta_{ll'}\rho^1]\} j_l(\omega r) j_{l'}(\omega r'), \quad (3.12)$$

where

$$c_j(x) = \frac{j_{j-1/2}(x)h_{j-1/2}^{(1)}(x) - j_{j+1/2}(x)h_{j+1/2}^{(1)}(x)}{j_{j-1/2}^2(x) - j_{j+1/2}^2(x)} \quad (3.13)$$

and

$$d_j(x) = \frac{i/x^2}{j_{j-1/2}^2(x) - j_{j+1/2}^2(x)} \quad (3.14)$$

and $x = \omega R$.

To summarize, the Dirac cavity partial-wave propagator is given by

$$S_{jll'm}(r, r', \omega) = -i\omega^2 [\delta_{ll'}\rho^3 + (l' - l)\rho^2] f_l(\omega r) f_{l'}(\omega r') + i\omega^2 \{c_j(x) [\delta_{ll'}\rho^3 + (l' - l)\rho^2] + d_j(x) [(\bar{l} - l)\delta_{ll'} - i\delta_{ll'}\rho^1]\} j_l(\omega r) j_{l'}(\omega r'). \quad (3.15)$$

B. The analytic structure of the propagator

The partial-wave propagators S_{jll}^0 and S_{jll} are defined in the lower-half ω plane by a generalization of the Schwartz reflection relation:

$$S_{jll}(r, r', \omega^*) = \rho^3 S_{jll}^0(r', r, \omega)^\dagger \rho^3, \tag{3.16}$$

derived in Appendix B. From this it is possible to determine the nature of the singularities in S_{jll} on the real axis.

The free partial-wave propagator, S_{jll}^0 , has a cut on the entire real axis with discontinuity

$$\begin{aligned} S_{jll}^0(r, r', \omega_0 + i\epsilon) - S_{jll}^0(r, r', \omega_0 - i\epsilon) \\ = -2i\omega_0^2 [\delta_{ll}\rho^3 + (l' - l)\rho^2] j_l(\omega_0 r) j_{l'}(\omega_0 r'). \end{aligned} \tag{3.17}$$

The Feynman boundary conditions require this cut to be displaced infinitesimally from the real axis, as shown in Fig. 4.

The full cavity propagator has no cut, only poles at the eigenstates of the Dirac cavity Hamiltonian. The poles occur at the zeros of the denominators of $c_j(x)$ and $d_j(x)$:

$$D_j(x) = j_{j-1/2}^2(x) - j_{j+1/2}^2(x), \tag{3.18}$$

which the reader will recognize as the current eigenvalue condition.² The residues of these poles are the properly normalized cavity wave functions. The Feynman boundary conditions require the poles to be displaced, as shown in Fig. 5.

The behavior of $S_{jll}(r, r', \omega)$ for large ω in the upper

half plane is as follows. $S_{jll}^0(r, r', \omega)$ is exponentially bounded,

$$\begin{aligned} S_{jll}^0(r, r', \omega) \sim -\frac{i}{2rr'} [\delta_{ll}\rho^3 + (l' - l)\rho^2] \\ \times e^{i\omega(r_> - r_<) - i\pi(l_> - l_<)/2}, \end{aligned} \tag{3.19}$$

except at $r = r'$, where it approaches a constant. In Eq. (3.19), $l_> = l$ if $r_> = r$ and $l_> = l'$ if $r_> = r'$. The boundary term \tilde{S}_{jll} vanishes exponentially for large $|\omega|$ except when $r = r' = R$,

$$\begin{aligned} \tilde{S}_{jll}(r, r', \omega) \sim -\frac{i}{2rr'} [2(j - l)\delta_{ll} - i\delta_{ll}\rho'] \\ \times e^{i\omega(2R - r - r') - i\pi(2j - l - l')/2}. \end{aligned} \tag{3.20}$$

Note only the $d_j(x)$ term of Eq. (3.15) contributes to Eq. (3.20). The $c_j(x)$ term vanishes faster by a power of $1/\omega^2$. The Dirac propagator is less well behaved at large ω than the scalar propagator reflecting its greater singularity at small relative time. Nevertheless, the large- ω behavior displayed in Eqs. (3.19) and (3.20) is sufficient to allow us to Wick rotate ω integration in the quark self-energy calculation of Sec. VI.

C. Multiple-reflection expansion

The multiple-reflection expansion for a Dirac propagator obeying Eq. (3.2) is derived in Ref. 16. We quote the result,

$$\begin{aligned} S(\vec{x}, \vec{x}', \omega) = S^0(\vec{x}, \vec{x}', \omega) + 2R^2 \int d\Omega_\alpha S^0(\vec{x}, \vec{\alpha}, \omega) P_\alpha S^0(\vec{\alpha}, \vec{x}', \omega) \\ + (2R^2)^2 \int d\Omega_\alpha d\Omega_\beta S^0(\vec{x}, \vec{\alpha}, \omega) P_\alpha S^0(\vec{\alpha}, \vec{\beta}, \omega) P_\beta S^0(\vec{\beta}, \vec{x}', \omega) + \dots, \end{aligned} \tag{3.21}$$

where

$$P_\alpha = \frac{1}{2}(1 + i\vec{\gamma} \cdot \hat{\alpha}). \tag{3.22}$$

D. Summing the multiple-reflection expansion

As in the scalar case, we substitute the partial-wave expansion, Eq. (3.6) for $S(\vec{x}, \vec{x}', \omega)$ and likewise for $S^0(\vec{x}, \vec{x}', \omega)$ into Eq. (3.21), and perform angular integrals using orthonormality properties of the $\phi_{jlm}(\Omega)$,

$$S_{jll}(r, r', \omega) = S_{jll}^0(r, r', \omega) + 2R^2 \sum_{l_1 l_2} S_{jll_1}^0(r, R, \omega) \sum_{n=0}^{\infty} [2R^2 P S^0(R, R, \omega) P]_{j_1 l_1 l_2}^n S_{j_2 l_2}^0(r, r', \omega). \tag{3.23}$$

S_{jll}^0 is a 2×2 matrix in ρ space. It is convenient to represent the l dependence ($l = j \pm \frac{1}{2}$) also in matrix form. In particular, $S_{jll}^0(r, r', \omega)$, given in Eq. (3.9), may be written as

$$S_j^0(r, r', \omega) = -i\omega^2 \begin{bmatrix} f_-(\omega r) \\ -i\rho^1 f_+(\omega r) \end{bmatrix} \rho^3 (f_-(\omega r'), -i\rho^1 f_+(\omega r')), \tag{3.24}$$

where $f_\pm(x) = f_{j \pm 1/2}(x)$, and the matrix displays the four combinations of l and l' values associated with each j . S_{jll}^0 has yet to be defined when $r = r' = R$. This problem is discussed at length in Ref. 16. With the correct definition of $S_{jll}^0(R, R, \omega)$ it is straightforward to perform the sum in Eq. (3.23) and obtain

$$\tilde{S}_j(r, r', \omega) = -\omega^2 x^2 [h_-^{(1)2}(x) - h_+^{(1)2}(x)] \begin{bmatrix} j_-(\omega r) \\ -i\rho^1 j_+(\omega r) \end{bmatrix} \frac{1 + k_j(x)\rho^3}{1 - k_j^2(x)} (j_-(\omega r'), -i\rho^1 j_+(\omega r')), \tag{3.25}$$

where $x = \omega R$, and

$$k_j(x) = -ix^2[h_-^{(1)}(x)j_-(x) - h_+^{(1)}(x)j_+(x)]. \quad (3.26)$$

A little algebra using the Wronskian identity

$$h_-^{(1)}(x)j_+(x) - h_+^{(1)}(x)j_-(x) = i/x^2 \quad (3.27)$$

converts this to the expected form, Eq. (3.12). The MRE is generated by a geometric expansion of the factor $(1 + k_j \rho^3)/(1 - k_j^2)$. Odd reflections are proportional to 1, even reflections to $k_j \rho^3$. As before, any number of reflections can be separated for special treatment by partial expansion of this factor.

The convergence of the Dirac MRE depends on the magnitude of $k_j^2(x)$. If

$$|k_j(x)| < 1, \quad (3.28)$$

the MRE converges, otherwise not. As in the scalar case, it is easy to show that there are regions on the real- ω axis in which Eq. (3.28) is not satisfied, but that Eq. (3.28) is valid and the MRE converges everywhere on the imaginary- ω axis. The proof is similar to the scalar case and we omit it.

E. Short-distance singularities

The confined Dirac propagator is more singular at short distances than the confined scalar propagator. Furthermore, the structure of the singularities is complicated by the presence of spin. Our analysis mimics the scalar case. The leading short-distance singularity is the same as for a half-space. In the notation of Sec. II E, we have

$$S^0(x_1, x'_1, \vec{p}) = (i\gamma^1 \partial / \partial x_1 + \vec{p} \cdot \vec{\gamma}) \Delta^0(x_1, x'_1, \vec{p}). \quad (3.29)$$

Substituting this in Eq. (3.21) gives

$$S_{\text{HS}}^1(x_1, x'_1, \vec{p}) = -i\gamma^1 (i\gamma^1 \partial / \partial x_1 + \vec{p} \cdot \vec{\gamma}) \Delta^0(-x_1, x'_1, \vec{p}), \quad (3.30)$$

or transforming to (\vec{x}, ω) space,

$$\begin{aligned} S_{\text{HS}}^1(x_1, x'_1, \omega) &= -i\gamma^1 S^0(\vec{x}_R, \vec{x}'_R, \omega) \\ &= S^0(x, x'_R, \omega) i\gamma^1, \end{aligned} \quad (3.31)$$

which again can be understood in terms of propagation from an image charge.

Using the same approximation as in Sec. II E, the one-reflection term for \vec{x} and \vec{x}' both close to the spherical surface and $\text{Im}\omega > 0$ is

$$\begin{aligned} S^1(\vec{x}, \vec{x}', \omega) &\sim \left[i\omega \gamma^0 \vec{\gamma} \cdot \hat{x} \right. \\ &\quad \left. - (\xi R - i\vec{\sigma} \cdot \hat{x} \times \vec{x}') \frac{1}{t} \frac{d}{dt} \right] \Delta^0(t, \omega), \end{aligned} \quad (3.32)$$

where $\vec{\gamma} \cdot \hat{x} \equiv \gamma \cdot \hat{x}'$, $\vec{\sigma} = (i/2) \vec{\gamma} \times \vec{\gamma}$, $t = R(\xi^2 + \theta^2)^{1/2}$, and $\Delta^0(t, \omega)$ is given by the right-hand side of Eq. (2.36) (taking the upper sign).

Higher reflection terms are most easily studied using the partial-wave expansion with the angle θ between \vec{x} and \vec{x}' set to zero and ω kept fixed. From the addition theorem for spinor spherical harmonics,

$$\begin{aligned} \sum_m \phi_{jj\pm 1/2m}(\Omega) \phi_{jj\pm 1/2m}^\dagger(\Omega') \\ = \frac{1}{4\pi} [(j + \frac{1}{2}) P_l(z) \pm i \vec{\sigma} \cdot (\hat{x} \times \hat{x}') P_l'(z)], \end{aligned} \quad (3.33)$$

where $z = \hat{x} \cdot \hat{x}'$, and one derives the identities

$$\begin{aligned} \sum_m \phi_{jj\pm 1/2m}(\Omega) \phi_{jj\pm 1/2m}^\dagger(\Omega) &= \frac{2j+1}{8\pi}, \\ \sum_m \phi_{jj\pm 1/2m}(\Omega) \phi_{jj\mp 1/2m}^\dagger(\Omega) &= -\frac{2j+1}{8\pi} \vec{\sigma} \cdot \hat{x}, \end{aligned} \quad (3.34)$$

which together with the expression for S_j^0 and \tilde{S}_j in Eqs. (3.15) and (3.25) give the following behavior for $r \sim r'$:

$$S^0(r, r', \cos\theta = 1, \omega) \sim \frac{-1}{4\pi} \frac{\rho^2 \vec{\sigma} \cdot \hat{x}}{|r - r'|^2}, \quad (3.35)$$

and for $r \sim r' \sim R$:

$$S^1(r, r', 1, \omega) \sim \frac{1}{4\pi} \frac{1}{(R^2 - rr')^2}, \quad (3.36)$$

$$S^2(r, r', 1, \omega) \sim \frac{\omega}{8\pi R} \ln \left[1 - \frac{rr'}{R^2} \right] \rho^3 \vec{\sigma} \cdot \hat{x}. \quad (3.37)$$

Equations (3.36) and (3.32) coincide if we take $\theta = \omega = 0$. Notice that, as expected, the two-reflection term in this case has a linear rather than a logarithmic short-distance behavior, as evidenced by the factor ω .

IV. THE GAUGE FIELD

A. The cavity propagators

We denote the confined vector propagator as $D_{\mu\nu}(\vec{x}, \vec{x}', \omega)$ in frequency space, we work in the Feynman gauge and suppress color indices. The time-space components, D_{0k} , vanish, leaving $D_{00}(\vec{x}, \vec{x}', \omega)$ the propagator of timelike gluons, and $D(\vec{x}, \vec{x}', \omega)$ the (3×3) matrix propagator for spacelike gluons. In the Feynman gauge we also require a ghost propagator $g(\vec{x}, \vec{x}', \omega)$. All of these Green's functions obey inhomogeneous Helmholtz equations¹⁷

$$(\nabla^2 + \omega^2) D(\vec{x}, \vec{x}', \omega) = \delta^3(\vec{x} - \vec{x}') \mathbb{1}, \quad (4.1a)$$

$$(\nabla^2 + \omega^2) D_{00}(\vec{x}, \vec{x}', \omega) = -\delta^3(\vec{x} - \vec{x}'), \quad (4.1b)$$

$$(\nabla^2 + \omega^2) g(\vec{x}, \vec{x}', \omega) = -\delta^3(\vec{x} - \vec{x}'), \quad (4.1c)$$

where the the signs reflect well-known metric properties of gauge theories. Through this section we take $\text{Im}\omega > 0$. Continuation to $\text{Im}\omega < 0$ is straightforward and discussed below.

The boundary condition on $F_{\mu\nu}$,

$$n_\mu F^{\mu\nu} = 0, \quad (4.2)$$

is not sufficient to allow one to invert Eqs. (4.1) and must be augmented by an additional gauge-fixing boundary condition.¹⁸ A sufficient, additional condition,

$$n_\mu A^\mu = 0, \quad (4.3)$$

can be obtained from either the Euclidian function integral or Lagrangian formulation of the field theory.

The boundary conditions on D induced by Eqs. (4.2) and (4.3) can be written with the aid of projection operators

$$P_{\parallel} = \hat{x} \hat{x} \quad (4.4)$$

and

$$P_{\perp} = 1 - \hat{x} \hat{x} \quad (4.5)$$

in dyadic notation,

$$P_{\parallel} D(\vec{\alpha}, \vec{x}', \omega) = 0, \quad (4.6)$$

$$(1 + \partial_{\alpha}) P_{\perp} D(\vec{\alpha}, \vec{x}', \omega) = 0, \quad (4.7)$$

where ∂_{α} is defined by Eq. (2.20). Similar conditions hold when \vec{x}' is on the boundary. The boundary condition on D_{00} induced by Eq. (4.2) is Neumann

$$\partial_{\alpha} D_{00}(\vec{\alpha}, \vec{x}', \omega) = 0. \quad (4.8)$$

The ghost boundary conditions are somewhat more difficult to obtain,¹⁹ but are fixed by gauge invariance also to be Neumann,

$$\partial_{\alpha} g(\vec{\alpha}, \vec{x}', \omega) = 0. \quad (4.9)$$

The ghost and timelike propagators will be largely ignored for the remainder of this section since scalar propagators subject to Neumann boundary conditions have been discussed in Sec. II.

We now turn to the propagator for spacelike gluons defined by Eqs. (4.1), (4.6), and (4.7). We define a partial-wave expansion employing vector spherical harmonics, $\vec{Y}_{JLM}(\Omega)$,

$$D(\vec{x}, \vec{x}', \omega) = \sum_{JLL'M} D_{JLL'}(r, r', \omega) \times \vec{Y}_{JLM}(\Omega) \vec{Y}_{JL'M}^{\dagger}(\Omega), \quad (4.10)$$

where J, L , and M are summed over the expected ranges: $J=0, 1, 2, \dots$, $J-1 \leq L \leq J+1$ (except if $J=0$, when only $L=1$ occurs), and $-J \leq M \leq J$. We decompose $D_{JLL'}$ into a free propagator and a boundary term,

$$D_{JLL'}(r, r', \omega) = D_{JLL'}^0(r, r', \omega) + \tilde{D}_{JLL'}(r, r', \omega). \quad (4.11)$$

The free partial-wave propagator is a direct generalization of the free scalar propagator,

$$D_{JLL'}^0(r, r', \omega) = -i\omega \delta_{LL'} j_L(\omega r_{<}) h_L^{(1)}(\omega r_{>}), \quad \text{Im} \omega > 0, \quad (4.12)$$

$D_{JLL'}^0$ is diagonal in L because the wave equation is. The bag boundary conditions on $F^{\mu\nu}$ are not diagonal in L but are diagonal instead in a basis of transverse magnetic (TM), longitudinal (LONG), and transverse electric (TE) wave functions.⁴ $D(\vec{x}, \vec{x}', \omega)$ is therefore also diagonal in this basis. To make use of this we define new basis vectors $\vec{V}_{JM}^k(\omega, \vec{x})$ which are solutions to the Helmholtz equations, where k runs over the labels TM, LONG, and TE:

$$\vec{V}_{JM}^{\text{TM}}(\omega, \vec{x}) = \left[\frac{J+1}{2J+1} \right]^{1/2} f_{J-1}(\omega r) \vec{Y}_{JJ-1M}(\Omega) - \left[\frac{J}{2J+1} \right]^{1/2} f_{J+1}(\omega r) \vec{Y}_{JJ+1M}(\Omega), \quad (4.13)$$

$$\vec{V}_{JM}^{\text{LONG}}(\omega, \vec{x}) = \left[\frac{J}{2J+1} \right]^{1/2} f_{J-1}(\omega r) \vec{Y}_{JJ-1M}(\Omega) + \left[\frac{J+1}{2J+1} \right]^{1/2} f_{J+1}(\omega r) \vec{Y}_{JJ+1M}(\Omega), \quad (4.14)$$

$$\vec{V}_{JM}^{\text{TE}}(\omega, \vec{x}) = f_J(\omega r) \vec{Y}_{JJM}(\Omega), \quad (4.15)$$

where $f_J(\omega r)$ is defined by Eq. (3.10). We also define vectors $\vec{U}_{JM}^k(\omega, \vec{x}')$ in the same way but with $f_J(\omega r)$ replaced by $j_J(\omega r)$. $D^0(\vec{x}, \vec{x}', \omega)$ is diagonal in the (TM, LONG, TE) basis

$$D^0(\vec{x}, \vec{x}', \omega) = -i\omega \sum_{JMK} \vec{V}_{JM}^k(\omega, \vec{x}) \vec{V}_{JM}^{k\dagger}(\omega, \vec{x}') \quad (4.16)$$

and so is $\tilde{D}(\vec{x}, \vec{x}', \omega)$,

$$\tilde{D}(\vec{x}, \vec{x}', \omega) = i\omega \sum_{JMK} a_J^k(x) \vec{U}_{JM}^k(\omega, \vec{x}) \vec{U}_{JM}^{k\dagger}(\omega, \vec{x}'). \quad (4.17)$$

The coefficients $a_J^k(x)$ are adjusted so that $D(\vec{x}, \vec{x}', \omega)$ obeys the appropriate boundary conditions with the result that

$$a_J^{\text{TM}}(x) = h_J^{(1)}(x) / j_J(x), \quad (4.18a)$$

$$a_J^{\text{LONG}}(x) = h_J^{(1)'}(x) / j_J'(x), \quad (4.18b)$$

and

$$a_J^{\text{TE}}(x) = \frac{h_J^{(1)}(x) + x h_J^{(1)'}(x)}{j_J(x) + x j_J'(x)}, \quad (4.18c)$$

reflecting Dirichlet, Neumann, and mixed boundary conditions, respectively [see Eqs. (2.11a) and (2.11b)].

It is convenient for later manipulations to rewrite the boundary term on the basis of spherical harmonics as in Eq. (4.10). This may be accomplished by introducing a set of projection operators, $Q_{JLL'}^{\text{TM}}$, $Q_{JLL'}^{\text{LONG}}$, and $Q_{JLL'}^{\text{TE}}$, defined by

$$Q_J^{\text{TM}} = \frac{1}{2J+1} \begin{bmatrix} J+1 & 0 & -[J(J+1)]^{1/2} \\ 0 & 0 & 0 \\ -[J(J+1)]^{1/2} & 0 & J \end{bmatrix}, \quad (4.19)$$

$$Q_J^{\text{LONG}} = \frac{1}{2J+1} \begin{bmatrix} J & 0 & [J(J+1)]^{1/2} \\ 0 & 0 & 0 \\ [J(J+1)]^{1/2} & 0 & J+1 \end{bmatrix}, \quad (4.20)$$

$$Q_J^{\text{TE}} = \begin{bmatrix} 0 & 0 & 0 \\ 0 & 1 & 0 \\ 0 & 0 & 0 \end{bmatrix}. \quad (4.21)$$

Using these operators the results of Eqs. (4.13)–(4.18) can be combined into

$$\tilde{D}_{JLL'}(r, r', \omega) = i\omega [a_J^{\text{TM}}(x) Q_{JLL'}^{\text{TM}} + a_J^{\text{LONG}}(x) Q_{JLL'}^{\text{LONG}} + a_J^{\text{TE}}(x) Q_{JLL'}^{\text{TE}}] j_L(\omega r) j_L(\omega r'). \quad (4.22)$$

Note that for $J=0$ only the longitudinal mode contributes since Q_{011}^{LONG} is the only nonzero projection-operator ma-

trix element with $J=0$ and $L=L'=1$. This was to be expected: there are no monopole modes of a transverse vector field.

For completeness we record the partial-wave decompositions of the timelike gluon and ghost propagators, which are the same,

$$D_{00l}=g_l=i\omega \left[j_l(\omega r_<) h_l^{(1)}(\omega r_>) - \frac{h_l^{(1)'}(x)}{j_l'(x)} j_l(\omega r) j_l(\omega r') \right]. \quad (4.23)$$

The gluon propagator is, of course, gauge dependent. A gauge transformation will change the form of the longitudinal and timelike pieces of the propagator but will leave the physical transverse pieces unchanged. Thus our expressions for the TM and TE pieces in $D_{JLL'}$ are, after appropriate manipulation, identical to the transverse propagators quoted by others working in the Coulomb gauge.

B. Analytic structure of the propagator

The partial-wave cavity propagators $D_{JLL'}^0(r, r', \omega)$ and $D_{JLL'}(r, r', \omega)$ are, like their scalar counterparts, real analytic functions of ω defined in the lower-half ω plane by

$$D_{JLL'}^0(r, r', \omega^*) = D_{JLL'}^0(r, r', \omega)^* , \quad (4.24a)$$

$$D_{JLL'}(r, r', \omega^*) = D_{JLL'}(r, r', \omega)^* . \quad (4.24b)$$

Consequently, the free partial-wave propagator, $D_{JLL'}^0$, has

$$\begin{aligned} D_\lambda(\vec{x}, \vec{x}', \omega) = & D^0(\vec{x}, \vec{x}', \omega) + 2R \int d\Omega_\alpha D^0(\vec{x}, \vec{\alpha}, \omega) \vec{K}_\lambda^\alpha D^0(\vec{\alpha}, \vec{x}', \omega) \\ & + (2R)^2 \int d\Omega_\alpha d\Omega_\beta D^0(\vec{x}, \vec{\alpha}, \omega) \vec{K}_\lambda^\alpha D^0(\vec{\alpha}, \vec{\beta}, \omega) \vec{K}_\lambda^\beta D^0(\vec{\beta}, \vec{x}', \omega) + \dots , \end{aligned} \quad (4.25)$$

where

$$\vec{K}_\lambda^\alpha = (\lambda + \partial^\alpha) P_{||}^\alpha - (1 + \partial_\alpha) P_{\perp}^\alpha . \quad (4.26)$$

As explained in detail in Ref. 16, the parameter λ is arbitrary. In order to resum the MRE, however, it is convenient to choose $\lambda=2$.

D. Summing the multiple-reflection expansion

If we substitute the partial-wave expansion for $D^0(\vec{x}, \vec{x}', \omega)$, analogous to Eq. (4.10), into the MRE and perform the angular integrations, the result is an infinite geometrical series involving a 3×3 matrix in L space ($L=J-1, J, J+1$) which is difficult to sum. Knowing that the full cavity propagator is diagonal in the TM, LONG, and TE basis, we attempt instead to substitute the expansion, Eq. (4.16), of $D^0(\vec{x}, \vec{x}', \omega)$ in this basis. We are confronted with integrals of the form

$$\int d\Omega_\alpha \vec{V}_{JM}^{\dagger k}(\omega, \vec{\alpha}) \vec{K}_\lambda^{\alpha} \vec{V}_{J'M'}^{k'}(\omega, \vec{\alpha}) = \delta_{JJ'} \delta_{MM'} C_{J\lambda}^{kk'}(x) , \quad (4.27)$$

where k and k' range over the labels TM, LONG, and TE

a cut along the entire real- ω axis which is displaced, as in Fig. 4. The full cavity partial-wave propagator, D_{JLL} , is a meromorphic function with poles at the values of ω corresponding to cavity eigenvalues of the TM [$j_J(x)=0$], TE [$j_J(x)+xj_J'(x)=0$], and LONG [$j_J'(x)=0$] modes. The poles are displaced, as in Fig. 5. There is a single, important exception to this: The timelike and ghost propagators obey Neumann boundary conditions and therefore have poles for $J=0$ at $\omega=0$, because $j_0'(x)$ vanishes at $x=0$. Had we worked in the Coulomb gauge, this effect would have required special treatment, as in Ref. 4. In covariant gauges there is no problem: In Appendix A, we show that the residue of the pole at $\omega=0$ in the lowest-order quark self-energy is proportional to the total color charge of the state, which for confined systems is zero. We believe this to be a general property of all Feynman graphs so that it is consistent merely to ignore the pole at $\omega=0$ throughout the calculation. The interested reader should consult Appendix A for a careful discussion.

Finally, we note that asymptotic behavior of the confined vector propagator as $|\omega| \rightarrow \infty$ in the complex plane coincides exactly with that of the confined scalar propagators.

C. Multiple-reflection expansion

As in the previous sections, we only quote the final expressions for the MRE. The results for D_{00} and g are given in Sec. II C so only D is new,

and the vectors, \vec{V}^k , are defined in Eqs. (4.13)–(4.15).

If and only if $\lambda=2$, then $C_{J\lambda}^{kk'}$ is proportional to $\delta^{kk'}$. That is to say, for $\lambda=2$ the polarization (either TM, LONG, or TE) is preserved by reflection. Since λ is, in fact, arbitrary we cannot assign any physical meaning to this property; nevertheless it facilitates summation of the MRE. Setting $\lambda=2$, we compute $C_{J,\lambda=2}^{kk'}$:

$$\begin{aligned} C_{J,\lambda=2}^{\text{TM, TM}}(x) = & j_J(x) h_J^{(1)}(x) \\ & + \frac{x}{2} [j_J(x) h_J^{(1)'}(x) + j_J'(x) h_J^{(1)}(x)] , \end{aligned} \quad (4.28a)$$

$$C_{J,\lambda=2}^{\text{LONG, LONG}}(x) = -\frac{x}{2} [j_J(x) h_J^{(1)'}(x) + j_J'(x) h_J^{(1)}(x)] , \quad (4.28b)$$

$$C_{J,\lambda=2}^{\text{TE, TE}}(x) = -C_{J,\lambda=2}^{\text{TM, TM}}(x) , \quad (4.28c)$$

and $C_{J,\lambda=2}^{kk'}=0$ when $k \neq k'$. With this choice of λ , the MRE, Eq. (4.25), simplifies to three independent geometrical series which may be summed to give the surface term $a_J^k(x)$ in the (TM, LONG, TE) basis [see Eq. (4.17)]

$$a_J^{\left[\begin{smallmatrix} \text{TE} \\ \text{TM} \end{smallmatrix} \right]}(x) = \frac{\pm 2ixh_j^{(1)}(x)[h_j^{(1)}(x) + xh_j^{(1)'}(x)]}{1 \pm 2ixh_j^{(1)}(x)j_j(x) \pm ix^2[h_j^{(1)}(x)j_j'(x) + h_j^{(1)'}(x)j_j(x)]}, \quad (4.29a)$$

$$a_J^{\text{LONG}}(x) = \frac{2ix^2h_j^{(1)}(x)h_j^{(1)'}(x)}{1 + ix^2[h_j^{(1)}(x)j_j'(x) + h_j^{(1)'}(x)j_j(x)]} \quad (4.29b)$$

for $\text{Im}\omega > 0$. To convert these results to the form we obtained earlier it is necessary to use the Wronskian identity, Eq. (2.25). The multiple-reflection expansion (with $\lambda=2$) is obtained by expanding the denominators in Eqs. (4.29) in geometrical series, allowing us to isolate any number of reflections for explicit, analytic treatment.

The convergence properties of the gluon MRE are similar to the scalar ME: it converges for all imaginary ω except at $\omega=0$.

E. Short-distance singularities

The short-distance singularity structure of the confined vector propagator D is easily derived from the properties of the scalar propagators into which it has been decomposed. As an example, the leading singularity of the one-reflection term is given by

$$D^1(\vec{x}, \vec{x}', \omega) \sim -(1 - 2P_{\parallel})\Delta^0(\vec{x}, \vec{x}', \omega). \quad (4.30)$$

V. FEYNMAN RULES

A. General considerations

With propagators in hand it is now straightforward to spell out the Feynman rules for a general confined field theory of scalar, spinor, and gauge vector fields. To be specific, we restrict our attention to confined QCD with massless quarks. We ignore the coupling to weak, electromagnetic or any other unconfined interactions. Restoring masses and external couplings is a straightforward procedure which will be carried out as necessary in future papers in this series. We generally omit the counterterm Lagrangian required for renormalization, although a mass counterterm is introduced and discussed in Sec. VI.

Unlike propagators, interaction vertices are *local* functions and consequently are not modified by the introduction of boundary conditions. It is possible therefore, simply to take the usual free-space Feynman rules in coordinate space and replace the free propagators everywhere by their confined counterparts.

For field theories confined to a spherical cavity, the coordinate-space Feynman rules are not the most convenient ones since they exploit neither the time-translation invariance nor the spherical symmetry. Time-translation invariance allows us to go over to a mixed (\vec{x}, ω) formulation, trading the time integration at each vertex for a frequency (energy) integration in each loop. In ordinary field theories momentum integrations in loops replace the spatial integrations at the vertices. In confined field theories this is not entirely possible. Rotational invariance allows us to replace the angular integration at the vertices by summations over the angular momenta around the loop. However, the radial integrations at each vertex remain. Conservation of angular momentum yields a Kronecker δ for the z components of angular momentum, but only a

weaker restriction on the total angular momentum j , namely that the j values at each vertex add to zero by the rules for addition of angular momentum.

In ordinary field theory, momentum integrations can be put into one-to-one correspondence with loops. In a spherical cavity the same can be done for the frequency integrations and for the sums over the z components of angular momentum, but not for the total angular momentum because the restriction on j values flowing into a vertex is not sufficient to reduce the number of independent j 's to one per loop.

It is now possible to give an "overview" of the Feynman perturbation theory. The general topology of graphs is the same as ordinary Feynman perturbation theory. The only exception to this is the need to distinguish between time-like and spacelike gluons. Each internal line carries a frequency ω , a total angular momentum j , and its z component, m . Orbital angular momentum quantum numbers, which are not conserved for spinors and vectors, appear on each end of such lines. Likewise, ρ -space indices appear on each end of Dirac propagators and radial coordinates at each end of all propagators. External lines carry a definite ω , j , and m into or out of the graph. They carry orbital angular momentum, which is summed, and contribute radial wave functions to the radial integrations at the vertices to which they couple.

Each vertex includes, in addition to a radial ($r^2 dr$) integration, a Wigner coefficient (or, for four-particle vertices, a combination of Wigner coefficients) expressing angular momentum conservation, and a "reduced vertex" factor reflecting the nature of the interaction which depends on the total angular momentum, orbital angular momentum, and Dirac ρ -space labels, but not on the z component of angular momentum.

The sums over internal m values can be performed explicitly leaving n -point functions which are spherical tensors depending only on external m values (e.g., the m dependence of a three-point function resides in a single Wigner coefficient). In the following subsections we discuss the vertices and external line factors which occur in QCD (Secs. VB and VC), and then summarize the Feynman rules in a form intended for practical use (Sec. VD).

B. Vertices

Here we discuss some general features of the vertices which occur in QCD, and assemble some results of angular integrations for later use. The complete vertices are enumerated with the rest of the rules below.

We work in a Feynman gauge where the effective Lagrangian is given by

$$\begin{aligned} \mathcal{L} = & -\frac{1}{4}F_{\mu\nu}^a F^{\mu\nu a} - \frac{1}{2}(\partial_\mu A_a^\mu)^2 - (\partial^\mu C_a^\dagger) D_\mu^{ab} C_b \\ & + i\bar{\psi}_j \gamma^\mu D_\mu^{jk} \psi_k, \end{aligned} \quad (5.1)$$

where

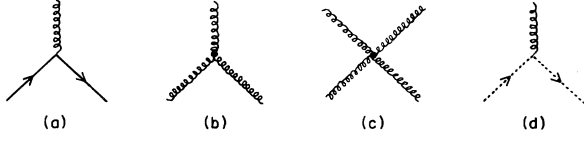


FIG. 6. QCD vertices: (a) quark-gluon, (b) three-gluon, (c) four-gluon, (d) ghost-gluon.

$$D_{\mu}^{ab} = \delta^{ab} \partial_{\mu} - g f^{abc} A_{\mu}^c, \quad (5.2)$$

$$D_{\mu jk} = \delta_{jk} \partial_{\mu} - ig T_{jk}^a A_{\mu}^a, \quad (5.3)$$

$$F_{\mu\nu}^a = \partial_{\mu} A_{\nu}^a - \partial_{\nu} A_{\mu}^a + g f^{abc} A_{\mu}^b A_{\nu}^c, \quad (5.4)$$

f^{abc} are the structure constants of the gauge group, and T_{ij}^a the generators in the fundamental representation. For $SU(3)$ $T_{ij}^a = \frac{1}{2} \lambda_{ij}^a$. Together with the appropriate boundary conditions, the Lagrangian in Eq. (5.1) implies the propagators given in the earlier sections. The vertices are derived from the interaction part of the Lagrangian

$$\mathcal{L}_{\text{int}}^{\text{eff}} = \mathcal{L}_{\bar{q}qg} + \mathcal{L}_{3g} + \mathcal{L}_{4g} + \mathcal{L}_{\text{ghost}} \quad (5.5)$$

with

$$\mathcal{L}_{\bar{q}qg} = g T_{ij}^a \bar{\psi}_i \gamma_{\mu} A^{\mu a} \psi_j, \quad (5.6a)$$

$$\mathcal{L}_{3g} = -g f^{abc} (\partial_{\mu} A_{\nu}^a) A^{\mu b} A^{\nu c}, \quad (5.6b)$$

$$\mathcal{L}_{4g} = -\frac{g^2}{4} f^{eab} f^{ecd} A_{\mu}^a A_{\nu}^b A^{\mu c} A^{\nu d}, \quad (5.6c)$$

$$\mathcal{L}_{\text{ghost}} = -g f^{abc} (\partial_{\mu} C_a^{\dagger}) A^{\mu b} C_c, \quad (5.6d)$$

and the standard graphical notation for QCD interaction vertices is summarized in Fig. 6. Our notation for vertices in a spherical cavity is summarized in Fig. 7.

Our major concern here is the procedure for performing the angular integrations at the vertices. The partial wave expansions of the propagators reduce the angular integrations at each vertex to an integral over products of three (or in the case of the four-gluon vertex, four) ordinary, spinor, or vector spherical harmonics. The specific interaction is reflected by the appearance of factors such as $i\vec{\gamma} \equiv -\vec{\sigma}\rho^2$ (at the fermion-spacelike gluon vertex) or $\vec{\nabla}$ (at the spacelike three-gluon or ghost-gluon vertices). An unavoidable complication of the partial-wave decomposition is the necessity to assign a “sense” (an arrow) to all lines, not just fermion and ghost lines as in ordinary field theory. The sense labels which end of the line carries the spherical harmonic (Y_{JM} , ϕ_{jlm} , or \vec{Y}_{JLM}) and which carries the adjoint spherical harmonic (Y_{JM}^* , ϕ_{jlm}^{\dagger} , or \vec{Y}_{JLM}^{\dagger}). The rules for assigning sense do differ, however, between gluons, on the one hand, and quarks or ghosts on the other. The sense arrows for the latter are, as usual, restricted

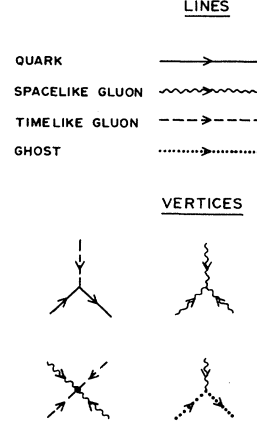


FIG. 7. Lines and vertices for QCD in a spherical cavity.

so that one line “enters” and one “leaves” every vertex. For gluons there is no such restriction, and the sense of any gluon line can be chosen arbitrarily. In this subsection we consider lines with sense chosen for convenience of illustration. The most general cases are enumerated with the rest of the rules. To simplify notation we introduce a coordinate-free representation for the spherical harmonics

$$Y_{JLM}^k(\Omega) = \langle \Omega k | L 1 J M \rangle, \quad (5.7a)$$

$$\phi_{jlm}^{\alpha}(\Omega) = \langle \Omega \alpha | l \frac{1}{2} j m \rangle, \quad (5.7b)$$

$$Y_{JM}(\Omega) = \langle \Omega | J 0 J M \rangle. \quad (5.7c)$$

First we consider three-particle vertices. These include quark and ghost coupling to spacelike and timelike gluons, and also three-gluon vertices, which may involve three spacelike, two spacelike plus one timelike, and one spacelike plus two timelike gluons. A three-timelike-gluon vertex does not occur. In general, these vertices are of the form

$$V = \langle l_2 s_2 j_2 m_2 | O_{l_2 j_2 m_2} | l_1 s_1 j_1 m_1 \rangle, \quad (5.8)$$

where O is an irreducible tensor operator. We apply the Wigner-Eckart theorem

$$V = (-1)^{j_2 - m_2} \begin{pmatrix} j_2 & j & j_1 \\ -m_2 & m & m_1 \end{pmatrix} \langle l_2 s_2 j_2 || O_{l_2 j_2} || l_1 s_1 j_1 \rangle \quad (5.9)$$

to remove the m dependence and define a “reduced vertex.” The only vertex operators which occur in QCD are Y_{JM} , $\vec{Y}_{JLM} \cdot \vec{\sigma}$, and $\vec{Y}_{JLM} \cdot \vec{\nabla}$. Their reduced matrix elements can be calculated using standard methods,

$$\langle l_2 s_2 j_2 || Y_J || l_1 s_1 j_1 \rangle = \frac{(-1)^{s+j_1+J}}{[4\pi(2s+1)]^{1/2}} \begin{bmatrix} l_2 & j_2 & s \\ j_1 & l_1 & J \end{bmatrix} \begin{pmatrix} l_2 & J & l_1 \\ 0 & 0 & 0 \end{pmatrix}, \quad (5.10)$$

$$\langle l_2 \frac{1}{2} j_2 || \vec{Y}_{JL} \cdot \vec{\sigma} || l_1 \frac{1}{2} j_1 \rangle = \frac{(-1)^{l_2}}{\sqrt{8\pi}} \begin{bmatrix} l_2 & l_1 & L \\ \frac{1}{2} & \frac{1}{2} & 1 \\ j_2 & j_1 & J \end{bmatrix} \begin{pmatrix} l_2 & L & l_1 \\ 0 & 0 & 0 \end{pmatrix}, \quad (5.11)$$

$$\begin{aligned}
 (l_2 s j_2 || \vec{Y}_{JL} \cdot \vec{\nabla} || l_1 s j_1) = & (-1)^{s+j_1+L} \left[\frac{(2j_1+1)(2j_2+1)}{12\pi(2l_1+1)} \right]^{1/2} \begin{Bmatrix} l_2 & j_2 & s \\ j_1 & l_1 & J \end{Bmatrix} \\
 & \times \left\{ \sqrt{l_1} \begin{pmatrix} L & l_2 & l_1-1 \\ 0 & 0 & 0 \end{pmatrix} \begin{bmatrix} L & J & 1 \\ l_1 & l_1-1 & l_2 \end{bmatrix} \left[\frac{\partial}{\partial r} + \frac{l_1+1}{r} \right] \right. \\
 & \left. - \sqrt{l_1+1} \begin{pmatrix} L & l_2 & l_1+1 \\ 0 & 0 & 0 \end{pmatrix} \begin{bmatrix} L & J & 1 \\ l_1 & l_1+1 & l_2 \end{bmatrix} \left[\frac{\partial}{\partial r} - \frac{l_1}{r} \right] \right\}. \tag{5.12}
 \end{aligned}$$

The spin, s , in Eq. (5.10) may be 0, $\frac{1}{2}$, or 1, while in Eq. (5.12) only 0 and 1 occur since there are no derivative couplings involving the quarks. The symbols in square brackets are related to conventional $6j$ and $9j$ symbols²⁰:

$$\begin{bmatrix} j_1 & j_2 & j_3 \\ j_4 & j_5 & j_6 \end{bmatrix} = \prod_{i=1}^6 (2j_i+1)^{1/2} \begin{Bmatrix} j_1 & j_2 & j_3 \\ j_4 & j_5 & j_6 \end{Bmatrix} \tag{5.13}$$

and correspondingly for the $9j$ symbols in square and curly brackets.

Four-gluon vertices are somewhat more complicated since there are many ways to couple four angular momenta to a scalar. The m dependence cannot be put into a single Wigner coefficient. Instead, two are required and they always appear in the same manner. For example, a vertex with four gluon lines carrying $J_1 \cdots J_4$ and $M_1 \cdots M_4$ into the vertex carries a factor

$$\sum_{JM} \begin{pmatrix} J_1 & J_2 & J \\ M_1 & M_2 & M \end{pmatrix} \begin{pmatrix} J_3 & J_4 & J \\ M_3 & M_4 & -M \end{pmatrix} (-1)^M V_J. \tag{5.14}$$

The coefficient V_J is independent of M and $M_1 \cdots M_4$, but depends on J and all other labels ($L_1 \cdots L_4, J_1 \cdots J_4$, and color) carried by the gluon lines. In analogy with the Wigner-Eckart theorem, we call V_J a reduced vertex. The four-gluon reduced vertices fall into two classes: (1) the couplings of two timelike and two spacelike gluons and, (2) the coupling of four spacelike gluons. The reduced vertices are determined by the angular integration of products of four spherical harmonics (ordinary or vector as the case may be) which we record here for future use. First we define the reduced vertices V_J^{ST} and V_J^{SS}

$$\int d\Omega Y_{J_1 M_1} Y_{J_2 M_2} \vec{Y}_{J_3 L_3 M_3} \cdot \vec{Y}_{J_4 L_4 M_4} = \sum_{JM} \begin{pmatrix} J_1 & J_2 & J \\ M_1 & M_2 & M \end{pmatrix} \begin{pmatrix} J_3 & J_4 & J \\ M_3 & M_4 & -M \end{pmatrix} (-1)^M V_J^{ST}(J_1 \cdots J_4, L_3, L_4), \tag{5.15a}$$

$$\int d\Omega \vec{Y}_{J_1 L_1 M_1} \cdot \vec{Y}_{J_2 L_2 M_2} \vec{Y}_{J_3 L_3 M_3} \cdot \vec{Y}_{J_4 L_4 M_4} = \sum_{JM} \begin{pmatrix} J_1 & J_2 & J \\ M_1 & M_2 & M \end{pmatrix} \begin{pmatrix} J_3 & J_4 & J \\ M_3 & M_4 & -M \end{pmatrix} (-1)^M V_J^{SS}(J_1 \cdots J_4, L_1 \cdots L_4). \tag{5.15b}$$

A straightforward calculation gives

$$V_J^{ST}(J_1 \cdots J_4, L_3, L_4) = \frac{(-1)^{J_3+L_4+J}}{4\pi\sqrt{3}} (2J_1+1)(2J_2+1)(2J+1) \begin{pmatrix} J_1 & J_2 & J \\ 0 & 0 & 0 \end{pmatrix} \begin{pmatrix} L_3 & L_4 & J \\ 0 & 0 & 0 \end{pmatrix} \begin{bmatrix} J_3 & J_4 & J \\ L_4 & L_3 & 1 \end{bmatrix}, \tag{5.16a}$$

$$V_J^{SS}(J_1 \cdots J_4, L_1 \cdots L_4) = \frac{(-1)^{J_1+L_2+J_3+L_4}}{12\pi} \begin{pmatrix} L_1 & L_2 & J \\ 0 & 0 & 0 \end{pmatrix} \begin{pmatrix} L_3 & L_4 & J \\ 0 & 0 & 0 \end{pmatrix} \begin{bmatrix} J_1 & J_2 & J \\ L_2 & L_1 & 1 \end{bmatrix} \begin{bmatrix} J_3 & J_4 & J \\ L_4 & L_3 & 1 \end{bmatrix}. \tag{5.16b}$$

The precise role of these reduced vertices in building the four-gluon vertices will be apparent in the rules which follow.

C. External wave functions

In order to specify rules for external lines in the cavity Feynman diagrams, we convert well-known expressions for cavity eigenfunctions into our notation. Color labels are standard. We suppress them.

Solutions to the Dirac equation in a spherical cavity are

labeled by four quantum numbers: a radial quantum number n , j and m —the total angular momentum and its z component—and parity. The last of these is often replaced by Dirac's quantum number κ . Instead we will replace it by l , the orbital angular momentum of the upper component of the Dirac spinor. For any value of $j, l = j \pm \frac{1}{2}$. The parity of a particle state is $(-1)^l$, that of an antiparticle is $(-1)^{l+1}$. Thus, for example, the state with $j = \frac{1}{2}, l = 0$ reduces to the $s_{1/2}$ mode in the nonrelativistic limit, while the $j = \frac{1}{2}, l = 1$ reduces to the $p_{1/2}$ mode. The eigenfrequency, ω_{njl} , is the n th root of the equation

$$j_l(x_{njl}) - 2(j-l)j_l(x_{njl}) = 0, \quad (5.17)$$

where $x_{njl} = \omega_{njl}R$, and $\bar{l} = j \mp \frac{1}{2}$ when $l = j \pm \frac{1}{2}$. In this notation the quark and antiquark wave functions can be written

$$\psi_{njlm}(\vec{x}) = \sum_{l'} \chi_{njll'}(r) \phi_{j'l'm}(\Omega), \quad (5.18)$$

where l' is summed over $j \pm \frac{1}{2}$. The radial wave function χ is a spinor in ρ space given by

$$\chi_{njll'}(r) = N_{njll'}(\omega_{njl}r) [\delta_{ll'} - \rho^2(\bar{l}-l)\delta_{\eta'}] u, \quad (5.19)$$

where $u = \begin{pmatrix} 1 \\ 0 \end{pmatrix}$ for quarks for $u = \begin{pmatrix} 0 \\ 1 \end{pmatrix}$ for antiquarks. The normalization constant $N_{njll'}$ is given by

$$N_{njll'}^{-2} = 2R^3 j_l^2(x_{njl}) \frac{x_{njl} - 2(j-l)(j+\frac{1}{2})}{x_{njl}}. \quad (5.20)$$

The Dirac conjugate wave function, $\bar{\chi} = \chi^\dagger \gamma^0$, is given by

$$\begin{aligned} \bar{\chi}_{njll'}(r) &= N_{njll'}(\omega_{njl}r) \\ &\times \bar{u} [\delta_{ll'} + \rho^2(\bar{l}-l)\delta_{\eta'}], \end{aligned} \quad (5.21)$$

where $\bar{u} \equiv u^\dagger \rho^3$.

Gluon wave functions are handled similarly with the aid of the projection operators defined in Sec. IV:

$$\vec{A}_{nJM}^{\text{TM(TE)}}(\vec{x}) = \sum_L \phi_{nJL}^{\text{TM(TE)}}(r) \vec{Y}_{JLM}(\Omega), \quad (5.22)$$

where

$$\phi_{nJL}^{\text{TE}}(r) = N_{nJ}^{\text{TE}} j_L(\omega_{nJ}r) (Q_J^{\text{TE}})_{JL} \quad (5.23a)$$

and

$$\phi_{nJL}^{\text{TM}}(r) = \frac{2J+1}{\sqrt{J}} N_{nJ}^{\text{TM}} j_L(\omega_{nJ}r) (Q_J^{\text{TM}})_{J+1,L}. \quad (5.23b)$$

The eigenfrequency conditions are

$$\frac{d}{dr} [r j_J(\omega_{nJ}r)]_{r=R} = 0 \quad (5.24a)$$

and

$$j_J(\omega_{nJ}R) = 0. \quad (5.24b)$$

The normalization constants are

$$(N_{nJ}^{\text{TE}})^{-2} = R^2 j_J^2(x_{nJ}^{\text{TE}}) \left[x_{nJ}^{\text{TE}} - \frac{J(J+1)}{x_{nJ}^{\text{TE}}} \right], \quad (5.25a)$$

$$(N_{nJ}^{\text{TM}})^{-2} = R^2 (2J+1) x_{nJ}^{\text{TM}} j_{J-1}^2(x_{nJ}^{\text{TM}}), \quad (5.25b)$$

where $x_{nJ}^{\text{TE(TM)}} = \omega_{nJ}^{\text{TE(TM)}} R$.

D. The rules

We collect the results of this and previous sections, and formulate a set of Feynman rules for confined QCD perturbation theory. First, however, we must specify to what amplitudes these rules apply. We consider Heisenberg picture states which are superpositions of confined but noninteracting quarks and transverse gluons obeying bag boundary conditions on a static spherical surface. Only global color singlets are allowed. We identify these states as eigenstates of the QCD Hamiltonian in the distant past or

future when the interaction has been adiabatically switched off, and call them in states and out states, respectively. Our rules apply to the calculation of the unitary transformation between in states and out states. More precisely, our rules apply to ‘‘S-matrix’’ elements defined by

$$\begin{aligned} \text{out} \langle 1 \cdots n | 1' \cdots n' \rangle_{\text{in}} &= 2\pi\delta \left[\sum_{i=1}^n \omega_i - \sum_{i=1}^{n'} \omega'_i \right] \\ &\times S(\omega_i j_i m_i, \omega'_i j'_i m'_i), \end{aligned} \quad (5.26)$$

where ω'_i, j'_i , and m'_i label incoming lines and ω_i, j_i , and m_i label outgoing lines. We have suppressed the extra labels (TE, TM; particle, antiparticle; parity and color) necessary to uniquely specify external lines. The relation between S and quantities of physical interest is straightforward and left to the reader. A specific example, the lowest-order quark self-energy, is described in the following section.

Our rules are as follows.

(1) *Diagrams.* Draw all topologically distinct one-particle-irreducible graphs using wiggly lines for spacelike gluons, dashed lines for timelike gluons, dotted lines for ghosts, solid lines for quarks and the three- and four-particle vertices shown in Fig. 7. Assign to each graph a statistical weight factor and a sign due to permutation of external quark lines, just as in ordinary QCD perturbation theory. Give *all* lines an arrow. The arrows on quark and ghost lines must be consistent throughout the graph (one quark or ghost entering and leaving each vertex). The arrows on gluon lines are arbitrary.

(2) *Labels.* Each external (quark or gluon) line carries energy (ω), radial quantum number (n), total angular momentum (j), z component (m), and orbital angular momentum (l). External gluon lines are labeled TE or TM. External quark lines are labeled with $l = j \pm \frac{1}{2}$ to specify their parity. Each loop is assigned a circulating energy (ω) and a z component of angular momentum (m). Then all internal lines are given energies (ω) and z components of angular momentum (m) consistent with conservation of ω and m at the vertices. Note that both m and ω are interpreted as *signed* quantities flowing in the direction of the arrows on all lines. Each internal line is given a total angular momentum (j). Internal spacelike gluon and quark lines are further labeled with orbital angular momentum l and l' at each end. All quark lines also carry ρ -space indices, and all lines carry color labels in the standard fashion all of which will be suppressed henceforth except where noted.

Each vertex carries a radial coordinate label (r).

(3) *Sums and integrals.* For each vertex an integral, $\int_0^R r^2 dr$. For each internal line a sum over all allowed j values. For each internal or external quark or spacelike gluon line, a sum over all l values consistent with j ($l = j \pm \frac{1}{2}$ for quarks, $l = J-1, J, J+1$ for gluons). For each loop an integral, $\int_{-\infty}^{\infty} d\omega/2\pi$, and a sum over all m values consistent with the current j values. All implicit ρ space and color labels are summed as usual.

(4) *Propagators.* For every internal line with its arrow pointing from a vertex labeled r' to one labeled r , i times a

full partial-wave propagator:

$$\begin{aligned} \text{quarks [Eq. (3.15)]:} & \quad iS_{jll'}(r, r', \omega), \\ \text{spacelike gluons [Eqs. (4.11)–(4.22)]:} & \quad iD_{JLL'}(r, r', \omega), \\ \text{timelike gluons [Eq. (4.23)]:} & \quad iD_{00J}(r, r', \omega), \\ \text{ghosts [Eq. (4.23)]:} & \quad ig_J(r, r', \omega) \end{aligned}$$

(see Fig. 8). Depending on the circumstances these may be decomposed into free and boundary parts, or any number of reflections and a remainder.

(5) *External lines. Quarks.* For each external line entering the graph (incoming quark or outgoing antiquark) carrying n, j, l and l' , a wave-function factor $\chi_{njll'}(r)$, and for each line leaving the graph (outgoing quark or incoming antiquark), a factor $\bar{\chi}_{njll'}(r) = \chi_{njll'}^*(r)$ [see Fig. 9(a)].

Gluons. For each external TE gluon carrying n, J , and L , a factor $\phi_{nJL}^{TE}(r)$. For each external TM gluon, a factor $\phi_{nJL}^{TM}(r)$ [see Fig. 9(b)].

(6) *Quark-gluon and ghost-gluon vertices.* For every such vertex in which the gluon is incoming, a factor

$$(-1)^{j_2 - m_2} \begin{pmatrix} j_2 & J & j_1 \\ -m_2 & M & m_1 \end{pmatrix}$$

times a reduced matrix element given in Figs. 10 or 11, where the labeling of angular momenta is given.

If the gluon is outgoing replace M by $-M$ and include a factor $(-1)^{J - M - L - S}$, where $S = 1$ for a spacelike gluon and $J - L - S = 0$ for a timelike gluon.

(7) *Three-gluon vertices.* Three types occur: three-spacelike, two-spacelike–one-timelike, and one-spacelike–two-timelike. In the first and last cases the vertex must be decomposed (keeping the labels on the legs fixed) as in Fig. 12 according to the leg on which the derivative acts (marked with a bar) and the leg with which the derivative is contracted (marked with a dot). For each vertex in which all gluons are incoming there is a factor

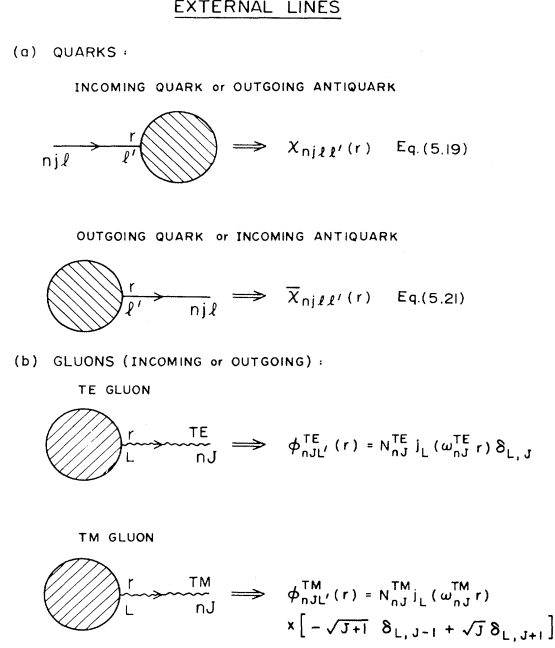


FIG. 9. External lines.

$$\begin{pmatrix} J_3 & J_2 & J_1 \\ M_3 & M_2 & M_1 \end{pmatrix}$$

times a reduced vertex given in Fig. 13, where the ordering of angular momenta is defined.

If the vertex involves any outgoing gluons, for each outgoing line change M_i to $-M_i$ and include a factor $(-1)^{J_i - M_i - L_i - S}$ as for the quark and ghost vertices.

(8) *Four-gluon vertices.* Two types occur: four-

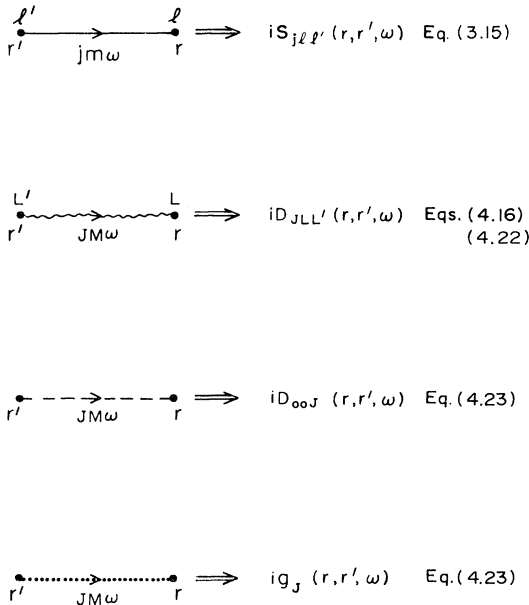


FIG. 8. Cavity propagators. Equation numbers refer to location in the text of explicit expressions for the propagators.

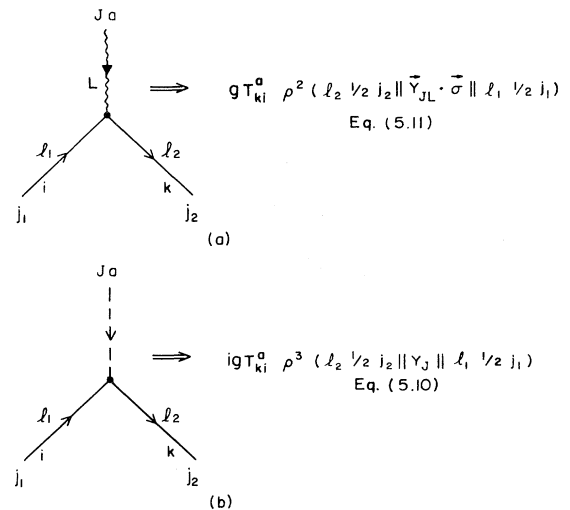


FIG. 10. Reduced quark-gluon vertices: (a) quark–spacelike-gluon, (b) quark–timelike-gluon. i, k , and a are color indices. Equation numbers refer to location in text of reduced matrix elements.

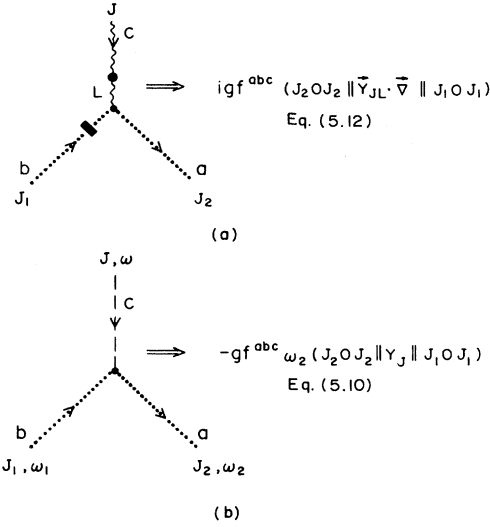


FIG. 11. Reduced ghost-gluon vertices: (a) ghost–spacelike-gluon, (b) ghost-timelike-gluon. Equation numbers refer to location in text of reduced matrix elements.

spacelike and two-spacelike–two-timelike. The former must be decomposed (keeping the labels on the legs fixed) as in Fig. 14, according to which pairs of legs are contracted over spatial indices. For each vertex there is a sum of the form

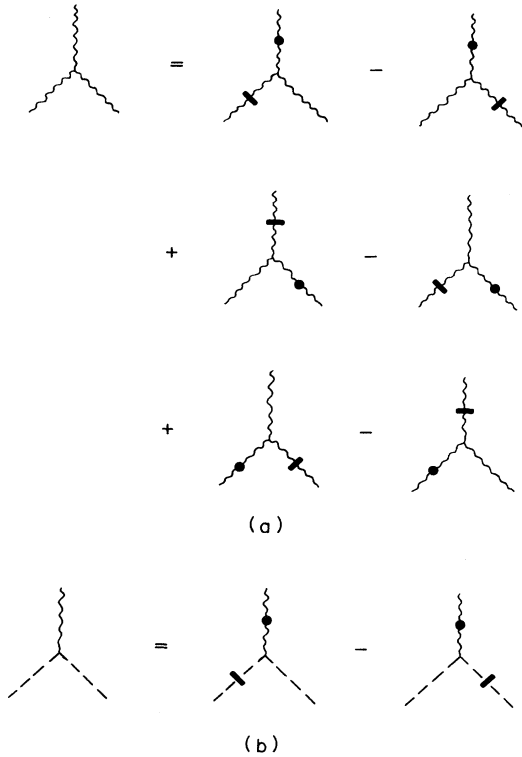


FIG. 12. Decomposition of the three-spacelike-gluon vertex (a), and the one-spacelike two-timelike gluon vertex (b), according to which leg is differentiated (marked with a bar) and which leg is contracted with the derivative (marked with a dot).

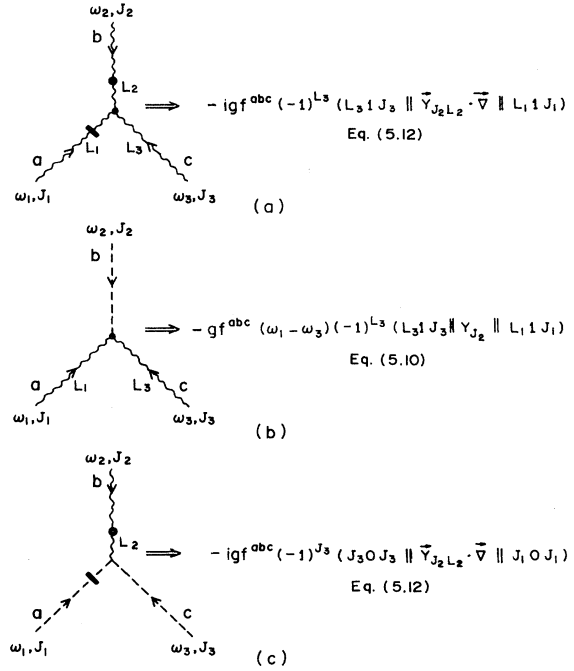


FIG. 13. Reduced three-gluon vertices: (a) three-spacelike, (b) two-spacelike, one-timelike, (c) one-spacelike, two-timelike. Equation numbers locate reduced matrix elements in text.

$$\sum_{JM} \binom{J_1 \ J_2 \ J}{M_1 \ M_2 \ M} \binom{J_3 \ J_4 \ J}{M_3 \ M_4 \ -M} (-1)^M$$

times a reduced matrix element given in Figs. 15.

As in the three-gluon vertices, if any vertex involves any outgoing gluons, for each outgoing line change M_i to $-M_i$ and include a factor $(-1)^{J_i - M_i - L_i - S}$.

(9) *Loops.* A factor (-1) for every ghost or quark loop.

VI. THE QUARK SELF-ENERGY

As an application of the rules and methods developed in the previous sections, we outline the calculation of the lowest-order quark self-energy in Feynman gauge QCD. At the end of the section we comment on the corresponding calculation for gluons. The contributing graphs are shown in Fig. 16. To isolate and renormalize potential ul-

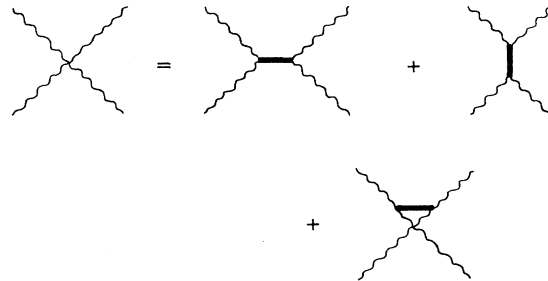


FIG. 14. Decomposition of the four-spacelike-gluon vertex according to which legs are contracted.

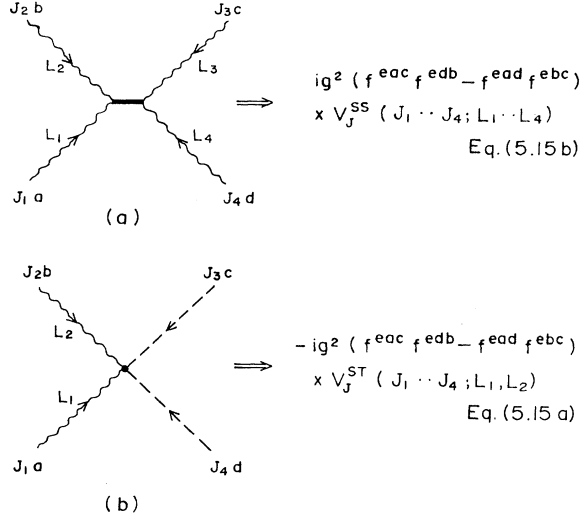


FIG. 15. Reduced four-gluon vertices: (a) four-spacelike gluons, (b) two-spacelike, two-timelike gluons. Equation numbers locate reduced vertices in text.

traviolet divergences, we decompose both the quark and gluon propagators into free and boundary terms:

$$S = S^0 + \tilde{S}, \quad (6.1a)$$

$$D = D^0 + \tilde{D}, \quad (6.1b)$$

$$D_{00} = D_{00}^0 + \tilde{D}_{00}. \quad (6.1c)$$

Likewise, we decompose the self-energy, $\tilde{\Sigma}_{njl}$, into two pieces

$$\Sigma_{njl} = \Sigma_{njl}^0 + \tilde{\Sigma}_{njl}, \quad (6.2)$$

where Σ_{njl}^0 contains only free propagators and $\tilde{\Sigma}_{njl}$ contains the rest. It turns out that all divergences lie in Σ_{njl}^0 . It can be shown that $\tilde{\Sigma}_{njl}$ is finite, although this is not ob-

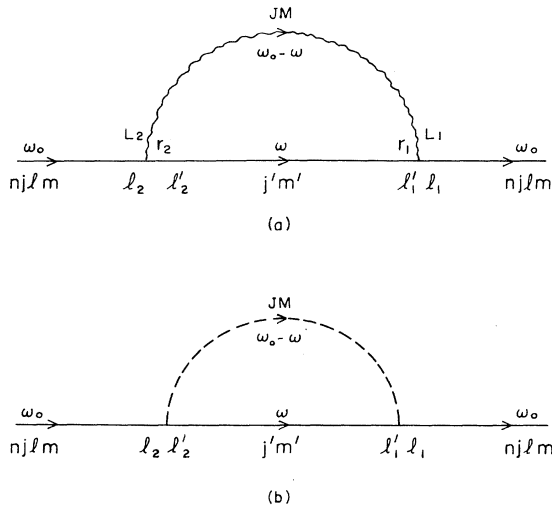


FIG. 16. Lowest-order diagrams for quark self-energy due to interaction with (a) spacelike gluon, (b) timelike gluon. $\omega_0 = \omega_{njl}$.

vious. Our analysis of the quark self-energy is divided into three parts. First we study Σ_{njl}^0 for both massless and massive quarks. For massless quarks we show that Σ_{njl}^0 is finite and unambiguous. For massive quarks we show that Σ_{njl}^0 is logarithmically divergent and that the logarithmic divergence can be absorbed into a state-independent renormalization of the quark mass. The renormalized quark mass obeys the same renormalization-group equation as in QCD without boundary conditions. Second, we show that $\tilde{\Sigma}_{njl}$ is finite. Third, we provide an explicit expression for $\tilde{\Sigma}_{njl}$ ready for numerical computation. The results of numerical calculation will be presented elsewhere.

A. Σ_{njl}^0

The contribution of free propagators to the quark self-energy is given by

$$\Sigma_{njl}^0 = ig^2 \int d^3x d^3x' dt \bar{\psi}_{njl}(\vec{x}, t) \gamma_\mu T^a S^0(\vec{x}, \vec{x}', t) \times \gamma_\nu T^a \psi_{njl}(\vec{x}', 0) D^{\mu\nu}(\vec{x}, \vec{x}', t), \quad (6.3)$$

where the spatial integrations extend only over the inside of the cavity. It is convenient to analyze this contribution in momentum space. We define a Fourier transform of the quark wave function,

$$\psi(\vec{x}, t) = \int \frac{d^3p}{(2\pi)^{3/2}} e^{i\vec{p}\cdot\vec{x}} \phi(\vec{p}) e^{-i\omega_0 t}. \quad (6.4)$$

Some important properties of $\phi(\vec{p})$ are given in Appendix C. We substitute the usual momentum-space representations of S^0 and $D^{0\mu\nu}$ along with Eq. (6.4) into Eq. (6.3). The result is

$$\Sigma_{njl}^0 = \int d^4p \bar{\phi}_{njl}(\vec{p}) \Sigma^0(p, m) \times \phi_{njl}(\vec{p}) \delta(p^0 - \omega_{njl}), \quad (6.5)$$

where $\Sigma^0(p, m)$ is the free-space, lowest-order self-energy in Feynman gauge, and m is the quark mass. $\Sigma^0(p, m)$ is logarithmically divergent and must be cut off. Employing Pauli-Villars regularization, we obtain²¹

$$\Sigma^0(p, m) = \frac{\alpha_s m}{\pi} \ln \Lambda^2 / p^2 - \frac{\alpha_s}{3\pi} (p - m) \ln \Lambda^2 / p^2 + \frac{4\alpha_s}{3\pi} \int_0^1 dz [m - p(1-z)/2] \times \ln \frac{p^2(1-z)}{m^2 z - p^2 z(1-z)}. \quad (6.6)$$

As shown in Appendix C, the quark equation of motion and boundary conditions yield

$$\int d^3p \bar{\phi}_{njl}(\vec{p}) (\not{p} - m) \phi_{njl}(\vec{p}) = 0, \quad (6.7)$$

so the second term in Eq. (6.6) gives a cutoff-independent contribution to Σ_{njl} .

For $m=0$ the first term in Eq. (6.6) is zero and we are left with a cutoff independent and finite result for Σ_{njl}^0 ,

$$\Sigma_{njl}^0 = \frac{\alpha_s}{3\pi} \int d^4p \bar{\phi}_{njl}(\vec{p}) \not{p} \ln p^2 \phi_{njl}(\vec{p}) \delta(p^0 - \omega_{njl}) \quad (6.8)$$

(the wave functions ϕ_{njl} fall sufficiently rapidly with $|\vec{p}|$ to make the integral convergent).

It should be emphasized that the result of Eq. (6.8) is not only finite but unambiguous. The quark self-energy in free space is linearly divergent and therefore subject to a possible finite ambiguity depending on the routing of momenta. The correct result, Eq. (6.8), is dictated by the Ward-Takahashi identity linking Σ to the vertex function. Calculations of the confined quark self-energy which do not handle the short-distance singularities analytically must be incorrect for this reason.²²

If the quark mass is not zero, Σ_{njl}^0 is divergent and must be renormalized. This may be done by adding a state-independent counterterm to the Lagrangian,

$$\mathcal{L} \rightarrow \mathcal{L} + \delta m \bar{\psi} \psi . \quad (6.9)$$

$$E_{njl} = E_{njl}^0(m) + \frac{\alpha_s}{3\pi} \int d^3p \bar{\phi}_{njl}(\vec{p})(p-4m)\phi_{njl}(\vec{p}) \ln p^2/\mu^2 + \frac{4\alpha_s}{3\pi} \int d^3p \bar{\phi}_{njl}(\vec{p}) \left[\int_0^1 dz \left[m - \frac{p(1-z)}{2} \right] \ln \frac{p^2(1-z)}{m^2z - p^2z(1-z)} \right] \phi_{njl}(\vec{p}) + \tilde{\Sigma}_{njl} , \quad (6.12)$$

where $E_{njl}^0 = (\omega_{njl}^2 + m^2)^{1/2}$ is the zeroth-order energy and $p^0 = \omega_{njl}$.

E_{njl} must be independent of the arbitrary renormalization point μ :

$$\frac{dE}{d\mu} = \frac{\partial E}{\partial \mu} + \frac{dm}{d\mu} \frac{\partial E}{\partial m} = 0 . \quad (6.13)$$

This is guaranteed by the renormalization-group equation obeyed by m ,

$$\frac{d \ln m}{d \ln \mu^2} = -\frac{\alpha_s}{\pi} , \quad (6.14)$$

which follows from Eq. (6.11), and the fact that the bare mass is independent of μ , and by the relation

$$\frac{dE_{njl}^0}{dm} = \int d^3p \bar{\phi}_{njl}(\vec{p}) \phi_{njl}(\vec{p}) . \quad (6.15)$$

Note it is not possible to define a quark mass renormalized ‘‘on shell’’ because cavity QCD does not possess any single-quark states. Nevertheless the quark mass is defined unambiguously both in principle and in practice by Eqs. (6.12) and (6.14). To make this clear imagine a fit to the hadron spectrum taking cavity QCD to order α_s . First one must choose μ , then fit m . The fit will be independent of μ up to $O(\alpha_s^2)$ corrections, but the value of m will depend on μ according to Eq. (6.14). As in ordinary perturbative QCD the $O(\alpha_s^2)$ differences between different renormalization schemes can only be settled by a full $O(\alpha_s^2)$ calculation. In the absence of such a calculation there is an arbitrariness associated with the choice of μ . We suppose that, as in asymptotic QCD, higher-order corrections will be minimized if μ is identified with some natural scale in the problem, e.g., by choosing

$$\int d^3p \bar{\phi}_{njl}(\vec{p}) \phi_{njl}(\vec{p}) \ln p^2/\mu^2 = 0$$

when analyzing the self-energy of a state with quantum numbers n, j, l .

This will give rise to a state-dependent contribution to the quark energy,

$$\Sigma_{njl}^{\text{CT}} = \delta m \int d^3p \bar{\phi}_{njl}(\vec{p}) \phi_{njl}(\vec{p}) , \quad (6.10)$$

so by taking

$$\delta m = -\frac{\alpha_s m}{\pi} \ln \Lambda^2/\mu^2 , \quad (6.11)$$

where μ is an arbitrary renormalization point, we can cancel the logarithmic divergence in Eq. (6.6). (We could of course equally well have started with a Lagrangian with a bare mass m_0 and then defined a renormalized mass m by $m = m_0 - \delta m$.) Combining Eqs. (6.6) and (6.11) gives

B. The finiteness of $\tilde{\Sigma}_{njl}$

To prove that $\tilde{\Sigma}_{njl}$ is finite, we proceed in two steps. First we argue by power counting that contributions with two or more reflections in either propagator are finite. Second, we show that the most divergent term in the remaining three contributions is finite.

Let $\Sigma_{njl}^{(m,n)}$ denote the contribution to Σ_{njl} with m and n reflections in the quark and gluon propagators, respectively. Forgetting about spin and external wave functions, we consider

$$\Sigma^{(m,n)} \sim \int_{-\infty}^{\infty} d\omega \int_{\text{cavity}} d^3x d^3x' (\gamma^0 \omega + i \vec{\gamma} \cdot \vec{\nabla}) \times \Delta^m(\vec{x}, \vec{x}', \omega) \Delta^n(\vec{x}, \vec{x}', \omega) . \quad (6.16)$$

To avoid unnecessarily long equations in this section we will use a rather abbreviated (but sufficient) notation: we use the sign \sim to mean leading singular behavior up to constants and signs, and up to $\vec{\gamma}$ matrices and relative signs between different terms. In the notation of Sec. II C: $\Delta^0 \sim (\eta^2 + \theta^2)^{-1/2}$ and $\Delta^2 \sim \ln \xi$. The only possible singularities occur close to the surface where,

$$\int d^3x d^3x' \sim \int_0 d\xi \int_{-\xi/\sqrt{2}}^{\xi/\sqrt{2}} d\eta \int_0 d\theta^2 , \quad (6.17)$$

so

$$\Sigma^{(2,0)} \sim \int_0 d\xi \int_{-\xi/\sqrt{2}}^{\xi/\sqrt{2}} d\eta \int_0 d\theta^2 \int_0^\infty dx \left[x \ln \xi + \frac{1}{\xi} \right] \times \frac{e^{-x(|\eta| + \xi)}}{s} , \quad (6.18)$$

$$\Sigma^{(0,2)} \sim \int_0 d\xi \int_{-\xi/\sqrt{2}}^{\xi/\sqrt{2}} d\eta \int_0 d\theta^2 \int_0^\infty dx \left[x + \frac{1}{s} \right] \times \ln \xi \frac{e^{-x(|\eta| + \xi)}}{s} , \quad (6.19)$$

where $s = R(\eta^2 + \theta^2)^{1/2}$ and we transformed the ω integration into an $x = i\omega R$ integration via Wick rotation. Simple power counting now shows that both $\Sigma^{(2,0)}$ and $\Sigma^{(0,2)}$ are finite. Obviously, terms with more than two reflections are also finite. The crucial convergence factor $\int_{-\xi/\sqrt{2}}^{\xi/\sqrt{2}} d\eta \sim \xi$ comes from phase space. This factor will be present also in the terms $\Sigma_{njl}^{(1,0)}$, $\Sigma_{njl}^{(0,1)}$, and $\Sigma_{njl}^{(1,1)}$, so although the propagators in these terms have the same leading singularities as in $\Sigma_{njl}^{(0,0)}$ the total term is one power less divergent. One thus concludes that the one reflection terms are *potentially* logarithmically divergent. We now show that in fact *no* divergences are present in these terms because of (i) the remaining translational invariance in the directions parallel to the surface and in the time direction, and (ii) the property, $\bar{\psi}(\vec{x})\psi(\vec{x})=0$ for \vec{x} on the surface, obeyed by the cavity wave functions.

It is convenient to use the (x, \vec{p}) representation which corresponds to computing Σ in an infinite half space.²³ This procedure will suffice for the leading divergence. [The reader who is unhappy about momentum-space arguments can use the explicit asymptotic (\vec{x}, ω) expressions in Eqs. (3.32) and (4.30) to construct the proof. This method

is much more tedious.] First consider $\Sigma_{njl}^{(1,0)}$ and for clarity put $x_1 = r$,

$$\Sigma_{njl}^{(1,0)} \sim \int d^3\vec{p} \int^R dr \int^R dr' \bar{\phi}_{njl}(\vec{p}, r) \Sigma^{(1,0)}(r, r', \vec{p}) \times \phi_{njl}(\vec{p}, r), \quad (6.20)$$

where

$$\Sigma^{(1,0)}(r, r', \vec{p}) \sim \int d^3\vec{q} \gamma_\mu S^1(r, r', \vec{p} + \vec{q}) \times \gamma^\mu \Delta^0(r, r', \vec{q}). \quad (6.21)$$

By using Eqs. (3.30), it is easy to show that the (\vec{p} -independent) leading singularity is given by

$$\Sigma^{(1,0)}(r, r', \vec{p}) \sim \frac{\partial}{\partial r} \int d^3\vec{q} \Delta^1(r, r', \vec{q}) \Delta^0(r, r', \vec{q}). \quad (6.22)$$

In deriving Eq. (6.22), translational invariance enters via $\int d^3\vec{q} \vec{q} \cdot \vec{\gamma} f(|\vec{q}|) = 0$. Substituting the explicit expressions, Eqs. (2.30) and (2.31) in Eq. (6.22), the \vec{q} integration can be performed, and using the variables ξ and η and Fourier transforming back to (\vec{x}, ω) space, we finally get

$$\Sigma_{njl}^{(1,0)} \sim \int_0 d\vec{x}_1 d\vec{x}'_1 \int_0 d\xi \int_{-\xi/\sqrt{2}}^{\xi/\sqrt{2}} d\eta \bar{\psi}_{njl}(\vec{x}) \psi_{njl}(\vec{x}') / (\xi + |\eta|)^2 \quad (6.23)$$

As expected, we gain one power of convergence from phase space, but the integral still looks logarithmically divergent. However, for \vec{x} close to the surface, it is easy to show $\bar{\psi}_{njl}(\vec{x})\psi_{njl}(\vec{x}) \sim \xi$, so $\Sigma_{njl}^{(1,0)}$ is finite.²⁴

Using the same technique one can easily convince oneself that the same holds true for $\Sigma_{njl}^{(0,1)}$ and $\Sigma_{njl}^{(1,1)}$. This completes the demonstration that $\tilde{\Sigma}_{njl}$ is finite.

C. The form of $\tilde{\Sigma}_{njl}$

Having established that $\tilde{\Sigma}_{njl}$ is finite, we use the Feynman rules from Sec. V to evaluate the two graphs in Fig. 16. The one with a spacelike gluon gives

$$\begin{aligned} \tilde{\Sigma}_{njl}^{\text{spacelike}} = & i \int_{-\infty}^{\infty} \frac{d\omega}{2\pi} \int_0^R r_1^2 dr_1 \int_0^R r_2^2 dr_2 \sum \bar{\chi}_{njl_1}(r_1) (gT^a \rho^2) \\ & \times (-1)^{j-m} \begin{pmatrix} j & J & j' \\ -m & M & m' \end{pmatrix} (l_1 \frac{1}{2} j || \vec{Y}_{JL_1} \cdot \vec{\sigma} || l_1' \frac{1}{2} j') i S_{j'l_1' l_2}(r_1, r_2, \omega) \\ & \times (-1)^{j'-m'+J-M-L_2-1} \begin{pmatrix} j' & J & j \\ -m' & -M & m \end{pmatrix} (l_2' \frac{1}{2} j' || \vec{Y}_{JL_2} \cdot \vec{\sigma} || l_2 \frac{1}{2} j) (gT^a \rho^2) \\ & \times \chi_{njl_2}(r_2) i D_{JL_1 L_2}(r_1, r_2, \omega_0 - \omega), \end{aligned} \quad (6.24)$$

where all internal j 's (i.e., J and j') and m 's (i.e., M and m') as well as *all* l 's (i.e., $l_1, l_2, l_1', l_2', L_1$, and L_2) consistent with angular momentum conservation are summed. For notational simplicity we put $\omega_{njl} = \omega_0$. The quark and gluon propagators are labeled generically in this equation. To construct $\tilde{\Sigma}$ we sum over contributions from $S^0 \otimes \bar{D}$, $\bar{S} \otimes D^0$, and $\bar{S} \otimes \bar{D}$ as defined in Eq. (6.1). The color algebra and sums on m can be performed

$$\begin{aligned} \tilde{\Sigma}_{njl}^{\text{spacelike}} = & -\frac{4i}{3} g^2 (2j+1)^{-1} \\ & \times \int_{-\infty}^{\infty} \frac{d\omega}{2\pi} \int_0^R r_1^2 dr_1 \int_0^R r_2^2 dr_2 \sum \delta(jJj') \bar{\chi}_{njl_1}(r_1) \\ & \times \rho^2 S_{j'l_1' l_2}(r_1, r_2, \omega) \rho^2 \chi_{njl_2}(r_2) D_{JL_1 L_2}(r_1, r_2, \omega_0 - \omega) \\ & \times (-1)^{J+j+j'-L_2} (l_1 \frac{1}{2} j || \vec{Y}_{JL_1} \cdot \vec{\sigma} || l_1' \frac{1}{2} j') \\ & \times (l_2' \frac{1}{2} j' || \vec{Y}_{JL_2} \cdot \vec{\sigma} || l_2 \frac{1}{2} j), \end{aligned} \quad (6.25)$$

where $\frac{4}{3}$ comes from the color sum, and $\delta(jJj')$ enforces the ‘‘triangular’’ condition that j' and J must be able to couple to j . The summation in Eq. (6.25) includes all allowed j and l values.

As stated, we wish to perform the ω integration by Wick rotating to the imaginary ω axis. The integrand in Eq. (6.25) has poles in the complex plane as shown in Fig. 17. Note that the poles in D have been shifted by ω_0 . Because of this a number of poles in the upper half plane may have been shifted to the right of the imaginary axis. For this to occur it is necessary that $\omega_0 \geq 2.08/R$, which is the energy of the pole in $D_{JLL}(r, r', \omega)$ closest to the imaginary axis. For quarks in the ground state $\omega_0 = 2.04/R$ and no poles cross the imaginary axis. We will confine our attention to this case in the remainder of the section.

To rotate the contour we must show that the circle at infinity in the complex ω plane can be ignored. From Eqs. (2.17), (2.18), (3.19), and (3.20), it appears that the integrand in Eq. (6.25) is exponentially damped at large $|\omega|$ except when $r = r'$, for free propagators, or $r = r' = R$, for boundary terms. These possible problem points have zero measure in the r integrations and therefore are benign. As an example, consider the case of the free-gluon propagator multiplying the quark boundary term for $\text{Im}\omega > 0$ in the limit $|\omega| \rightarrow \infty$,

$$\tilde{S}(r, r', \omega) D^0(r, r', \omega_0 - \omega) \sim \frac{1}{\omega} e^{i\omega(2R - r - r') + i\omega(r_> - r_<)} . \quad (6.26)$$

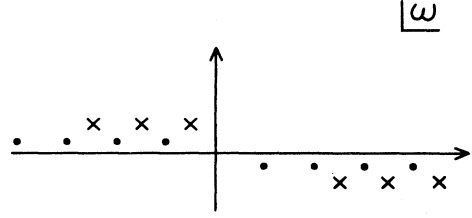


FIG. 17. Singularities in the complex ω plane corresponding to the graph in Fig. 16(a). Dots and crosses denote poles in $S_{j'l'_2}(r_1, r_2, \omega)$ and $D_{JL_1L_2}(r_1, r_2, \omega_0 - \omega)$, respectively.

Since the behavior near $r = r' = R$ is our only concern we look only at

$$\int_0^R dr' \int_0^R dr \frac{1}{\omega} e^{i\omega(2R - r - r') + i\omega(r_> - r_<)} \sim \frac{1}{|\omega|^3} . \quad (6.27)$$

The contribution of the circle arc at infinity therefore vanishes like $1/|\omega|^2$. The same analysis can be carried through for the circle arc in the lower half plane.

We are thus justified in rotating the contour to the imaginary axis,

$$\begin{aligned} \tilde{\Sigma}_{nj'l}^{\text{spacelike}} &= \frac{16\pi\alpha_s}{3(2j+1)} \int_{-\infty}^{\infty} \frac{d\eta}{2\pi} \int_0^R r_1^2 dr_1 \int_0^R r_2^2 dr_2 \sum \delta(jJj') \bar{\chi}_{njll_1}(r_1) \\ &\quad \times \rho^2 S_{j'l'_1l'_2}(r_1, r_2, i\eta) \rho^2 \chi_{njll_2}(r_2) D_{JL_1L_2}(r_1, r_2, \omega_0 - i\eta) \\ &\quad \times (-1)^{j+J'+J-L_2} (l_1 \frac{1}{2} j || \vec{Y}_{JL_1} \cdot \vec{\sigma} || l'_1 \frac{1}{2} j') (l'_2 \frac{1}{2} j' || \vec{Y}_{JL_2} \cdot \vec{\sigma} || l_2 \frac{1}{2} j) , \end{aligned} \quad (6.28)$$

where we have put $\omega = i\eta$ and $\alpha_s = g^2/4\pi$. The same steps applied to the timelike-gluon diagram in Fig. 16(b) yields

$$\begin{aligned} \tilde{\Sigma}_{nj'l}^{\text{timelike}} &= \frac{16\pi\alpha_s}{3(2j+1)} \int_{-\infty}^{\infty} \frac{d\eta}{2\pi} \int_0^R r_1^2 dr_1 \int_0^R r_2^2 dr_2 \sum \delta(jJj') \bar{\chi}_{njll_1}(r_1) \\ &\quad \times \rho^3 S_{j'l'_1l'_2}(r_1, r_2, i\eta) \rho^3 \chi_{njll_2}(r_2) D_{00J}(r_1, r_2, \omega_0 - i\eta) \\ &\quad \times (-1)^{j+J'} (l_1 \frac{1}{2} j || Y_J || l'_1 \frac{1}{2} j') (l'_2 \frac{1}{2} j' || Y_J || l_2 \frac{1}{2} j) . \end{aligned} \quad (6.29)$$

Note that the pole at $\omega = 0$ in the timelike piece of the gluon propagator always crosses the imaginary axis. In rotating the ω contour to the imaginary axis, we pick up the residue at this pole. However, in accordance with the discussion in Appendix A this contribution to Σ is to be dropped. Equations (6.28) and (6.29) are our final results. Further evaluation must be numerical

To reiterate, Eqs. (6.28) and (6.29) should not be evaluated for the full quark and gluon propagators. Instead, the zero-reflection term must be separated out and evaluated analytically. The convergent remainder can be evaluated using the above expressions.

D. The gluon self-energy

The corresponding calculation for the gluon self-energy presents new problems. The graphs in Fig. 18 give the following expression for the no-reflection contribution to the gluon self-energy:

$$\Pi_{nJ}^0 = \int d^4p A_{nJ}^{i*}(\vec{p}) \Pi_{ij}^0(p) A_{nJ}^j(\vec{p}) \delta(p^0 - \omega_{nJ}) , \quad (6.30)$$

where the index TE(TM) is suppressed. In the dimensional-regularization scheme, $\Pi_{ij}^0(p)$ is given by²⁵

FIG. 18. Graphs contributing to the $O(\alpha_s)$ gluon self-energy.

$$\Pi_{ij}^0(p) = \frac{5\alpha_s}{4\pi} (p_i p_j - \delta_{ij} p^2) \left[-\frac{2}{\epsilon} + \ln \frac{-p^2}{\mu^2} \right], \quad (6.31)$$

where μ is an arbitrary mass scale and the presence of a pole $1/\epsilon$ signals a logarithmic singularity. In contrast to the quark case, the equations of motion do *not* imply that

$$\int d^3p A^i(\vec{p})(p_i p_j - g_{ij} p^2) A^j(\vec{p}) = 0.$$

In fact, it is not hard to show (using methods similar to those in Appendix C) that Π_{nJ}^0 , as given by Eqs. (6.30) and (6.31), is not well defined. The deep reason for this trouble is most likely that by using free propagators we violate gauge invariance which is responsible for converting the naive quadratic divergence in the gluon self-energy into a logarithmic one.

The divergence in Π_{nJ}^0 is consistent with the result of a similar calculation of the photon self-energy in confined scalar electrodynamics in Ref. 26. There it was shown that after defining a suitable regularization procedure, the divergent term in Π_{JL}^0 is found to cancel against divergent terms in the one- and two-reflection contributions, leaving a finite result. Our belief is that the same thing will happen for QCD in a sphere, i.e., when we include the reflection terms (and thus restore gauge invariance) the gluon self-energy will be finite.

ACKNOWLEDGMENTS

We thank our colleagues at the center for Theoretical Physics for discussions and suggestions. We are especially grateful to Ken Johnson for numerous valuable conversations. This work was supported in part through funds provided by the U.S. Department of Energy under Contract No. DE-AC02-76ER03069. The work of T.H.H. was supported in part by the Swedish Natural Science Research Council under Contract No. F-PD4728-103.

APPENDIX A: THE POLE AT $\omega=0$ IN $D_{00}(\vec{x}, \vec{x}', \omega)$

Here we analyze the pole at $\omega=0$ in the propagator for timelike gluons.⁷ We discuss its origins and show that it can be consistently neglected in the lowest-order self-energy for quarks in a cavity provided the state is a color singlet. We believe this to be a special case of the general result that this pole is to be systematically neglected in all cavity calculations involving color-singlet states.

The pole arises in the Neumann propagator because the Helmholtz equation

$$(\nabla^2 + \omega^2) \Delta^N(\vec{x}, \vec{x}', \omega) = \delta^3(\vec{x} - \vec{x}') \quad (A1)$$

becomes inconsistent with the boundary condition

$$\hat{n} \cdot \vec{\nabla} \Delta^N(\vec{x}, \vec{x}', \omega) \Big|_{\vec{x}=\vec{\alpha}} = 0 \quad (A2)$$

as $\omega \rightarrow 0$. To see the pole integrate Eq. (A1) over the cavity using Eq. (A2),

$$\int d^3x \Delta^N(\vec{x}, \vec{x}', \omega) = \frac{1}{\omega^2}. \quad (A3)$$

The residue of the pole is independent of \vec{x}' and, by symmetry, of \vec{x} . To obtain the residue, separate out the pole,

$$\Delta^N(\vec{x}, \vec{x}', \omega) = \frac{C}{\omega^2} + \bar{\Delta}^N(\vec{x}, \vec{x}', \omega), \quad (A4)$$

where $\bar{\Delta}^N$ is not singular as $\omega=0$. Substituting into Eq. (A3) and integrating over \vec{x}' we find

$$C = \frac{1}{V}, \quad (A5)$$

where V is the cavity volume, $4\pi/3R^3$ for a sphere.

The physical origin of the singularity lies in Gauss's law. Identifying \vec{E} with $-\vec{\nabla}\phi$, Eq. (A1) reduces, when $\omega \rightarrow 0$, to Gauss's law with a point charge at \vec{x}' , the integral form of which,

$$\oint \hat{n} \cdot \vec{E} ds = 1, \quad (A6)$$

is not consistent with the Neumann condition, Eq. (A2).

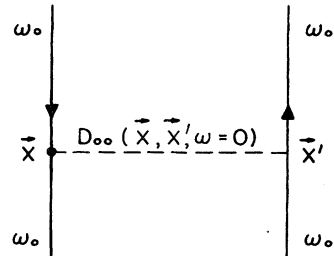
This singularity afflicts the propagator of timelike gluons and the ghost propagator in QCD. [Although longitudinal gluons also obey Neumann boundary conditions, the propagator is saved from this affliction by its vector character as can be seen by inspection of Eq. (4.14).]

Left unregulated, the singularity at $\omega=0$ would make individual Feynman graphs infinite. For example, the timelike gluon contribution to the lowest-order $\bar{q}q$ interaction energy, Fig. 19, carries no energy, so $\omega=0$. This infinity cancels against an infinity in the quark self-energy. To allow us to manipulate the graphs it is necessary to regulate the singularity. The obvious way is to introduce a mass, σ , which is subsequently taken to zero,

$$\frac{3}{4\pi R^3 \omega^2} \rightarrow \lim_{\sigma \rightarrow 0} \frac{3}{8\pi R^3} \left[\frac{1}{\omega^2 - \sigma^2 + i\epsilon} \right] \equiv K(\sigma, \omega). \quad (A7)$$

Now consider the contribution of the pole at $\omega=0$ to the lowest-order energy shift of any hadron. We keep σ finite throughout the calculation and let it pass to zero at the end. From exchange graphs such as Fig. 19, we obtain

$$\Delta E_{ij}(\sigma) \propto g^2 \vec{T}_i \cdot \vec{T}_j \int d^3x d^3x' \psi^\dagger(\vec{x}) \psi(\vec{x}) \times \psi^\dagger(x') \psi(x') K(\sigma, \omega) \quad (A8)$$

FIG. 19. $O(\alpha_s)$ contribution to the quark-antiquark interaction energy from exchange of a timelike gluon.

$$\propto -\frac{3g^2}{4\pi R^3\sigma^2}\vec{T}_i\cdot\vec{T}_j. \quad (\text{A9})$$

From the self-energy graphs, we obtain

$$\begin{aligned} \Delta E_i(\sigma) \propto g^2(\vec{T}_i)^2 \int \frac{d\omega}{2\pi} \int d^3x d^3x' \psi^\dagger(\vec{x}) iS(\vec{x}, \vec{x}', \omega) \\ \times \gamma^0 \psi(\vec{x}') K(\sigma, \omega_i - \omega), \end{aligned} \quad (\text{A10})$$

where ω_i is the energy of the external line. $S(\vec{x}, \vec{x}', \omega)$ contains a singularity at $\omega = \omega_i - i\epsilon$ with residue $\psi(\vec{x})\bar{\psi}(\vec{x}')$. The ω -integration contour is pinched near $\omega = \omega_i$ and is best performed closing in the upper half plane around the pole in $K(\sigma, \omega_i - \omega)$ at $\omega = \omega_i - \sigma + i\epsilon$ leaving

$$\begin{aligned} \Delta E_i(\sigma) \propto -\frac{3g^2}{8\pi R^3\sigma^2}\vec{T}_i^2 \int d^3x d^3x' \psi^\dagger(x)\psi(x) \\ \times \psi^\dagger(x')\psi(x') \end{aligned} \quad (\text{A11})$$

$$\propto -\frac{3g^2}{8\pi R^3\sigma^2}\vec{T}_i^2. \quad (\text{A12})$$

All other contributions to $\Delta E_i(\sigma)$ are finite as $\sigma \rightarrow 0$. For a given cavity state, Eq. (A9) is to be summed over all pairs and Eq. (A12) over all quarks with the result that

$$\Delta E(\sigma) = -\frac{3g^2}{8\pi R^3\sigma^2}\langle T^2 \rangle, \quad (\text{A13})$$

where

$$\langle T^2 \rangle = \left[\sum_i \vec{T}_i \right]^2 \quad (\text{A14})$$

is the quadratic Casimir constant of color SU(3). $\langle T^2 \rangle = 0$ for color singlets, completing our argument that the pole at $\omega = 0$ in D_{00} does not contribute to the self-energy to this order.

APPENDIX B: CAVITY DIRAC PROPAGATOR

We wish to construct the partial-wave expansions for the free Dirac propagator $S^0(\vec{x}, \vec{x}', \omega)$ and the boundary term $\tilde{S}(\vec{x}, \vec{x}', \omega)$. We work in the upper-half ω plane. It is convenient to expand both in partial waves and in ρ space:

$$\begin{aligned} S^0(\vec{x}, \vec{x}', \omega) &= \sum_{k=0}^3 \rho^k A^k(\vec{x}, \vec{x}', \omega) \\ &= \sum_{k=0}^3 \sum_{jll'm} \rho^k A_{jll'}^k(r, r', \omega) \phi_{jlm}(\Omega) \\ &\quad \times \phi_{j'l'm'}^\dagger(\Omega'), \end{aligned} \quad (\text{B1})$$

$$\begin{aligned} \tilde{S}(\vec{x}_1, \vec{x}'_1, \omega) &= \sum_{k=0}^3 \rho^k a^k(\vec{x}, \vec{x}', \omega) \\ &= \sum_{k=0}^3 \sum_{jll'm} \rho^k a_{jll'}^k(r, r', \omega) \phi_{jlm}(\Omega) \\ &\quad \times \phi_{j'l'm'}^\dagger(\Omega'), \end{aligned} \quad (\text{B2})$$

where $\rho^0 = 1$. S^0 is defined by Eq. (3.4) and appropriate boundary conditions at $r, r' = \infty$. Substituting Eq. (B1), we find

$$\omega A^3 - \vec{\sigma} \cdot \vec{\nabla} A^2 = \delta^3(\vec{x} - \vec{x}'), \quad (\text{B3a})$$

$$\omega A^2 + \vec{\sigma} \cdot \vec{\nabla} A^3 = 0, \quad (\text{B3b})$$

$$i\omega A^1 - \vec{\sigma} \cdot \vec{\nabla} A^0 = 0, \quad (\text{B3c})$$

$$i\omega A^0 - \vec{\sigma} \cdot \vec{\nabla} A^1 = 0. \quad (\text{B3d})$$

The $\{a^k\}$ obey analogous equations without any source.

The first step is to construct the free propagator. From Eqs. (B3a) and (B3b), we obtain

$$(\omega^2 + \nabla^2)A^3 = \omega \delta^3(\vec{x} - \vec{x}'), \quad (\text{B4})$$

$$A^2 = -\frac{\vec{\sigma} \cdot \vec{\nabla}}{\omega} A^3. \quad (\text{B5})$$

Equations (B3c) and (B3d), together with the Feynman boundary condition at $r, r' = \infty$, give $A^0 = A^1 = 0$. It follows immediately from Eq. (B4) that

$$A_{jll'}^3(r, r', \omega) = -i\omega^2 f_l(\omega r) f_{l'}(\omega r') \delta_{ll'}, \quad (\text{B6})$$

where $f_l(\omega r)$ is defined by Eq. (3.10). For definiteness we take $r > r'$, so $f_l(\omega r) = h_l^{(1)}(\omega r)$ and $f_{l'}(\omega r') = j_{l'}(\omega r')$. The operator $I = \vec{\sigma} \cdot \vec{\nabla} / \omega$ obeys $[I, \vec{J}] = 0$ and $\{I, P\} = 0$, where P is the parity operator. Furthermore, in the space of spinor solutions, $g_l(\omega r) \phi_{jlm}(\Omega)$, to the Helmholtz equation, $I^2 = -1$. From these properties it is easy to show that

$$I g_l(\omega r) \phi_{jlm}(\Omega) = (\bar{l} - l) g_l(\omega r) \phi_{j\bar{l}m}(\Omega) \quad (\text{B7})$$

in Eq. (B7), \bar{l} is defined by $\bar{l} = j \mp \frac{1}{2}$ when $l = j \pm \frac{1}{2}$. Using Eq. (B7), Eq. (B5) becomes

$$A_{jll'}^2(r, r', \omega) = -i\omega^2 (l' - l) f_l(\omega r) f_{l'}(\omega r'). \quad (\text{B8})$$

This completes the derivation of Eq. (3.9).

To determine the boundary term \tilde{S} , we must impose the boundary condition Eq. (3.5). In terms of the $\{A^k\}$ and $\{a^k\}$ we find

$$\begin{aligned} \vec{\sigma} \cdot \hat{x} a^0 - a^2 &= A^2, \\ \vec{\sigma} \cdot \hat{x} a^1 - i a^3 &= i A^3, \end{aligned} \quad (\text{B9})$$

when $r = R$. Because \tilde{S} obeys the homogeneous Dirac equation each of the components, $a^k(\vec{x}, \vec{x}', \omega)$ is a solution to the Helmholtz equation. Regularity at $r=0$ and $r'=0$ requires

$$a_{jll'}^k(r, r', \omega) = C_{jll'}^k j_l(\omega r) j_{l'}(\omega r'). \quad (\text{B10})$$

The operator $\vec{\sigma} \cdot \hat{x}$ merely interchanges l and \bar{l} :

$$\vec{\sigma} \cdot \hat{x} \phi_{jlm} = -\phi_{j\bar{l}m}. \quad (\text{B11})$$

Combining our results for A^k with our parametrization for a^k and with Eq. (B11), we obtain a set of equations for the $C_{jll'}^k$ from the boundary condition, Eq. (B9):

$$\begin{aligned} C_{jll'}^0 j_l(x) + C_{jll'}^2 j_l(x) &= i\omega^2 (l' - l) h_l^{(1)}(x), \\ C_{jll'}^1 j_l(x) + i C_{jll'}^3 j_l(x) &= -\omega^2 \delta_{ll'} h_l^{(1)}(x). \end{aligned} \quad (\text{B12})$$

Two additional constraints on the C^k follow from Dirac's equation:

$$\begin{aligned} a^2 &= -Ia^3, \\ a^1 &= -iIa^0, \end{aligned}$$

or, with the aid of Eq. (B7),

$$\begin{aligned} C_{jll'}^2 &= (\bar{I}-1)C_{jll'}^3, \\ C_{jll'}^1 &= i(\bar{I}-1)C_{jll'}^0. \end{aligned} \quad (\text{B13})$$

Equations (B12) and (B13) may be solved simultaneously for $C_{jll'}^k$ with the result that

$$\begin{aligned} C_{jll'}^0 &= i\omega^2 d_j(x)(\bar{I}-1)\delta_{ll'}, \\ C_{jll'}^1 &= \omega^2 d_j(x)\delta_{ll'}, \\ C_{jll'}^2 &= i\omega^2 c_j(x)(I'-1), \\ C_{jll'}^3 &= i\omega^2 c_j(x)\delta_{ll'}, \end{aligned} \quad (\text{B14})$$

where $c_j(x)$ and $d_j(x)$ are defined in Eqs. (3.13) and (3.14). This completes the derivation of Eq. (3.12).

Finally, we turn to the problem of defining $S(\vec{x}, \vec{x}', \omega)$ in the lower-half ω plane. In addition to Eq. (3.1), $S(\vec{x}, \vec{x}', \omega)$ also obeys

$$S(\vec{x}, \vec{x}', \omega)(\gamma^0 \omega - i\vec{\gamma} \cdot \vec{\nabla}') = \delta^3(\vec{x} - \vec{x}'). \quad (\text{B15})$$

If we take the conjugate of this equation and multiply by γ^0 on both sides, we obtain

$$(\gamma^0 \omega^* + i\vec{\gamma} \cdot \vec{\nabla}') \gamma^0 S^\dagger(\vec{x}', \vec{x}, \omega) \gamma^0 = \delta^3(\vec{x} - \vec{x}'). \quad (\text{B16})$$

The uniqueness of the Dirac propagator requires

$$\gamma^0 S^\dagger(\vec{x}', \vec{x}, \omega) \gamma^0 = S(\vec{x}, \vec{x}', \omega^*). \quad (\text{B17})$$

Expanding in partial waves and replacing γ^0 by ρ^3 , we obtain Eq. (3.16).

APPENDIX C: CAVITY DIRAC WAVE FUNCTIONS IN MOMENTUM SPACE

The cavity quark wave function $\psi(\vec{x})e^{-i\omega t}$ obeys

$$(i\partial - m)\psi = 0 \quad (\text{C1})$$

both inside and outside the cavity. Its Fourier transform, $\phi(p)$, does not obey $(\not{p} - m)\phi(\vec{p}) = 0$ ($p^0 = \omega$) because of the discontinuity in $\psi(x)$ at the surface. The proper Fourier transform space analog of Eq. (C1) is

$$\int d^3p \bar{\phi}(\vec{p})(\not{p} - m)\phi(\vec{p}) = 0. \quad (\text{C2})$$

To derive Eq. (C2), consider

$$I \equiv \int d^3x \bar{\psi}(\vec{x})(\gamma^0 \omega + i\vec{\gamma} \cdot \vec{\nabla} - m)\psi(\vec{x}). \quad (\text{C3})$$

Note that $\psi(\vec{x})$ obeys

$$(\omega \gamma^0 + i\vec{\gamma} \cdot \vec{\nabla} - m)\psi(\vec{x}) = 0, \quad r < R \quad (\text{C4a})$$

$$(i\hat{x} \cdot \vec{\gamma} + 1)\psi(\vec{x}) = 0, \quad r = R \quad (\text{C4b})$$

$$\psi(\vec{x}) = 0, \quad r > R. \quad (\text{C4c})$$

To be precise, define a continuous function $\Psi(\vec{x})$ which obeys Eqs. (C4a) and (C4b), but no Eq. (C4c). Then

$$\psi(\vec{x}) = \theta(R-r)\Psi(\vec{x}). \quad (\text{C5})$$

It is easy to see then that

$$(\omega \gamma^0 + i\vec{\gamma} \cdot \vec{\nabla} - m)\psi = i\vec{\gamma} \cdot \hat{x}\Psi\delta(r-R), \quad (\text{C6})$$

so I , defined by Eq. (C3), becomes

$$I = \int d^3x \bar{\psi}(x)i\vec{\gamma} \cdot \hat{x}\psi(\vec{x})\delta(r-R), \quad (\text{C7})$$

which vanishes as a consequence of Eq. (C4b). Fourier transforming, we obtain Eq. (C2).

For quarks with mass m , the cavity wave functions in Eqs. (5.18) to (5.20) are modified to

$$\psi_{njlm}(\vec{x}) = \sum_{l'} \chi_{njll'}(r)\phi_{jll'm}(\Omega), \quad (\text{C8})$$

$$\chi_{njll'}(r) = N_{njll'} j_{l'}(x\xi)$$

$$\times \left[\delta_{ll'} - \frac{x}{\alpha + \lambda} \rho^2 (\bar{I} - 1) \delta_{ll'} \right] u, \quad (\text{C9})$$

where $\lambda = mR$, $x = x_{njl}$, $\xi = r/R$, and $\alpha = (x^2 + \lambda^2)^{1/2}$. x_{njl} is the n th nontrivial, positive solution to

$$j_l(x) - \frac{2(j-l)x}{\alpha + \lambda} j_l(x) = 0 \quad (\text{C10})$$

and $N_{njll'}$ is given by

$$N_{njll'}^{-2} = 2R^3 j_l^2(x) \frac{\alpha[\alpha - 2(j-l)(j + \frac{1}{2})] + \lambda}{x^2}. \quad (\text{C11})$$

Using the addition theorem

$$e^{i\vec{p} \cdot \vec{x}} \delta^{\alpha\beta} = 4\pi \sum_{jlm} i^l j_l(pr) \phi_{jlm}^\alpha(\Omega_p) \phi_{jlm}^{\beta*}(\Omega_x), \quad (\text{C12})$$

where the sum is over all allowed j , l , and m values, the Fourier transform is performed by using the orthogonality of the spinor spherical harmonics, and the integral,

$$\begin{aligned} t_l(x, y) &\equiv \int_0^1 u^2 du j_l(xu) j_l(yu) \\ &= \frac{1}{x^2 - y^2} [y j_l(x) j_{l-1}(y) - x j_l(y) j_{l-1}(x)]. \end{aligned} \quad (\text{C13})$$

The result is identical in form to Eqs. (C8) and (C9), and reads

$$\phi_{njlm}(\vec{p}) = \sum_{l'} \xi_{njll'}(\vec{p}) \phi_{jll'm}(\Omega_p), \quad (\text{C14})$$

$$\begin{aligned} \xi_{njll'}(\vec{p}) &= R^3 \sqrt{2/\pi} (-i)^l N_{njll'} t_{l'}(x, pR) \\ &\times \left[\delta_{ll'} - \frac{x}{\alpha + \lambda} \rho^2 (\bar{I} - 1) \delta_{ll'} \right] u \end{aligned} \quad (\text{C15})$$

[note the Eq. (C13) holds for $l=0$ if $j_{-1} = -n_0$ is used].

- ¹A. Chodos, R. L. Jaffe, K. Johnson, C. B. Thorn, and V. F. Weisskopf, *Phys. Rev. D* **9**, 3471 (1974).
- ²A. Chodos, R. L. Jaffe, K. Johnson, and C. B. Thorn, *Phys. Rev. D* **10**, 2599 (1974); T. A. DeGrand, R. L. Jaffe, K. Johnson, and J. Kiskis, *ibid.* **12**, 2060 (1975).
- ³P. Vinciarelli, *Lett. Nuovo Cimento* **4**, 905 (1972); M. Creutz, *Phys. Rev. D* **10**, 1749 (1974); M. Creutz and K. S. Soh, *ibid.* **12**, 443 (1975); R. Friedberg and T. D. Lee, *ibid.* **15**, 1694 (1977); **16**, 1096 (1977).
- ⁴T. D. Lee, *Phys. Rev. D* **19**, 1802 (1979).
- ⁵For example, in Lee's model (see Ref. 4) it is necessary to introduce a coupling $\sim \sigma^2 A_\mu^a A^{\mu a}$ between the gluon and scalar fields in order that A_μ^a vanish outside the bag.
- ⁶F. E. Close and R. R. Horgan, *Nucl. Phys.* **B164**, 413 (1980); A. Maciel, D. Phil. thesis, Oxford University (unpublished); S. Monaghan, D. Phil. thesis, Oxford University (unpublished).
- ⁷S. A. Chin, A. K. Kerman, and X. H. Yang, *Nucl. Phys.* **A382**, 355 (1982).
- ⁸J. D. Breit, Columbia University Report No. CU-TP-229, 1982 (unpublished).
- ⁹O. Maxwell and V. Vento, Orsay Report No. IPNO/TH82-11, 1982 (unpublished).
- ¹⁰J. Baacke, Y. Igarashi, and G. Kasperidus, *Z. Phys. C* **17**, 161 (1983).
- ¹¹R. Balian and C. Bloch, *Ann. Phys. (N.Y.)* **60**, 401 (1970).
- ¹²C. Bender and P. Hayes, *Phys. Rev. D* **14**, 2622 (1976).
- ¹³K. A. Milton, *Phys. Rev. D* **22**, 1444 (1980).
- ¹⁴R. L. Jaffe and A. Patrascioiu, *Phys. Rev. D* **12**, 1314 (1975).
- ¹⁵R. Balian and C. Bloch, *Ann. Phys. (N.Y.)* **64**, 271 (1971).
- ¹⁶T. H. Hansson and R. L. Jaffe, MIT Report No. CTP 1070, 1983 (unpublished).
- ¹⁷We use the same sign conventions for propagators as in J. D. Bjorken and S. D. Drell, *Relativistic Quantum Fields* (McGraw-Hill, New York, 1965).
- ¹⁸The need for additional gauge fixing can be seen in the Euclidean functional integral. Consider, for example, an Abelian gauge theory. The usual, covariant gauge condition $\delta(\partial_\mu A^\mu - B)$ fails to fix the gauge because the four-dimensional Laplace's equation, $\nabla^2 \Lambda = 0$, possesses nontrivial solutions in a finite domain. The additional condition, $n_\mu A^\mu = 0$, is consistent with $n_\mu F^{\mu\nu} = 0$ and eliminates this remaining degeneracy. We thank Roscoe Giles for discussions on this subject.
- ¹⁹The boundary conditions for ghost fields on plane surfaces were derived by T. H. Hansson, K. Johnson, and C. Peterson, *Phys. Rev. D* **26**, 415 (1982). Using functional methods, they showed that ghost fields obey the same boundary conditions as those imposed by gauge invariance on an infinitesimal gauge transformation $\alpha_s(\vec{x})$. It is not hard to prove that if $A_\mu(\vec{x})$ obeys the boundary conditions corresponding to Eqs. (4.6)–(4.8) on a sphere, then for
- $$A_{\mu a}^a(\vec{x}) = A_{\mu a}(\vec{x}) - \partial_\mu \alpha_a(\vec{x}) + g f_{abc} \alpha_b(\vec{x}) A_{\mu c}(\vec{x})$$
- to obey the same boundary conditions, one must impose Neumann boundary conditions on $\alpha_a(\vec{x})$. Thus the ghost fields also obey Neumann boundary conditions on a sphere.
- ²⁰Our $3j$, $6j$, and $9j$ symbols are defined as in A. R. Edmonds, *Angular Momentum in Quantum Mechanics*, 2nd ed. (Princeton University Press, Princeton, New Jersey, 1960), which also contains formulas useful in deriving Eqs. (5.10)–(5.12).
- ²¹See, for example, J. D. Bjorken and S. D. Drell, *Relativistic Quantum Mechanics* (McGraw-Hill, New York, 1964), p. 163.
- ²²We thank Ken Johnson for emphasizing this point to us.
- ²³A similar problem for the electromagnetic energy shift of a confined quark was treated by A. Chodos and C. B. Thorn, *Phys. Lett.* **53B**, 359 (1974).
- ²⁴The cautious reader might worry that since potentially divergent terms canceled due to symmetric integrations, a numerical calculation could be dangerous. This would certainly be true if the canceling divergences had been linear, as in the case of the zero-reflection term. There the situation was saved by the Ward identities. In the present case the potential divergences are only logarithmic so the rearrangement of sums or the details of the numerical integration procedure should have no influence on the result.
- ²⁵C. Itzykson and J. B. Zuber, *Quantum Field Theory* (McGraw-Hill, New York, 1980).
- ²⁶T. H. Hansson, K. Johnson, and C. Peterson, *Phys. Rev. D* **26**, 415 (1982).